Reduced Folate Carrier 1 is Present in Retinal Microvessels and Contributes to the Regulation of the Inner Blood Retinal Barrier in Health and Retinal Ischemia

Gokce Gurler[1], Nevin Belder[2], Mustafa Caglar Beker[3], Melike Sever-Bahcekapili[1], Gokhan Uruk[1], Ertugrul Kilic[3], Muge Yemisci[1,4,5]

1. The Institute of Neurological Sciences and Psychiatry, Hacettepe University, Ankara, Turkey
2. Biotechnology Institute, Ankara University, Ankara, Turkey
3. Istanbul Medipol University, Physiology, Istanbul, Turkey
4. Faculty of Medicine, Department of Neurology, Hacettepe University, Ankara, Turkey
5. Neuroscience and Neurotechnology Center of Excellence (NÖROM) Ankara, Turkey

Corresponding Author:
Muge Yemisci (MD, PhD), Professor of Neurology
Institute of Neurological Sciences and Psychiatry, Hacettepe University, Ankara, Turkey
Faculty of Medicine, Department of Neurology, Hacettepe University, Ankara, Turkey
Neuroscience and Neurotechnology Center of Excellence (NÖROM) Ankara, Turkey
myemisciozkan@gmail.com

Abstract

The inner blood-retina barrier (BRB) resembles the blood-brain barrier (BBB) and is comprised of a single layer endothelium sealed with tight junctions whose abluminal surface is ensheathed by pericytes. The inner BRB is essential for providing a constant and controlled flow of nutrients and molecules to meet metabolic needs. Accordingly, the inner BRB harbors numerous carriers providing the exchange of molecules between blood and retina. One of these carriers is Reduced Folate Carrier 1 (RFC1), which functions as a folate transporter, and has been one of the most consistently detected genes in cerebral pericytes in a recent meta-analysis. The presence of RFC1 protein and its functions in retinal pericytes and microvessels have been overlooked so far despite the similarities between retinal and cerebral microcirculation. In this report, our purposes were to assess the presence of RFC1 protein in retinal microvessels and surrounding pericytes, and modify to increase or decrease RFC1 levels to explore its roles in healthy and ischemic retinal microvessels. Our analyses on whole mount retinas, and trypsin digest preparations from adult Swiss albino mice with concomitant pericyte and endothelial cell markers have shown the presence of RFC1 protein in the inner BRB and colocalization with pericytes. In vivo modifications of RFC1 expression levels were accomplished by intravitreal delivery of genetic and pharmacological agents. Knocking down RFC1 expression via custom-designed short interfering RNA (siRNA) resulted in microvascular dysfunction which was presented by the disintegration of tight junction proteins and the main basal membrane protein collagen-4. This was accompanied by extensive endogenous IgG extravasation suggesting impairment in the barrier functions. On the other hand, delivering RFC1 expressing lentiviral vector to overexpress RFC1 in the retina induced immunosignal increase in tight junction proteins and collagen-4 confirming the role of RFC1 in the inner BRB functions. Administration of methotrexate (MTX), the pharmacological competitive inhibitor of folate, resulted in increased levels of RFC1. In retinal ischemia models, one-hour retinal ischemia increased RFC1 levels and decreased collagen-4 and occludin levels. These effects could be partially reversed with pre-treatment by RFC1 expressing lentiviral vector. All these indicate the importance of RFC1 levels in the pathophysiology of retinal ischemia, a prevalent cause of blindness worldwide. In conclusion, our study clarifies the presence of RFC1 in inner BRB and offers a novel perspective on RFC1, other than being a folate carrier, as a regulator of inner BRB in healthy and ischemic retinas.

Keywords: RFC1, blood-retina barrier, retinal ischemia, siRNA, lentiviral vector, folate, MTX

Introduction

The retina is the extended and outwardly positioned part of the brain and is considered as the continuation of it anatomically. It has a blood-retina barrier (BRB) similar to the blood-brain barrier (BBB), which precludes the free transfer of substances from the capillary blood [1]. The BRB is composed of two compartments. The outer BRB is composed of the retinal pigmented epithelium (RPE), which are specialized epithelial cells sealed with tight junctions, residing between the neural retina and a fenestrated capillary network called the choriocapillaris. It partly functions to determine the transfer of nutrients from the choriocapillaris to the retina [2]. The inner BRB is established in the inner retinal microvessels and comprises specialized endothelial cells secured by tight junctions, enclosed by basal lamina, pericytes, and perivascular astrocytes; hence it resembles the BBB and is essential for the maintenance of homeostasis through its unique properties [1, 3]. Pericytes are a crucial element of both the BBB and the inner BRB, and have various roles including the regulation of microvascular blood flow, immunity, and barrier integrity in health and pathologic states such as ischemia, hence have increasingly been gaining attention [4-8].

Reduced Folate Carrier 1 (RFC1), also called solute carrier family 19 member 1 (SLC19a1), is one of the folate transporters present in mammalian cells. Importantly, RFC1 protein is present in the brain capillary endothelial cells of BBB and is involved in the transfer of folate to the brain parenchyma [9-12]. A handful of transcriptomic studies showed that RFC1 mRNA is one of the most consistently detected transcripts in cerebral microvascular mural cells (pericytes and vascular smooth muscle cells) [13], which could suggest the importance of RFC1 in their physiology. To date, in the retina, the expression of RFC1 and its transporter function for folate was primarily evaluated in the RPE, thus the outer BRB [14-17]. On the other hand, a single in vitro study demonstrated the presence of RFC1 mRNA in isolated rat retinal vascular endothelial cells [18], and another study focusing on the transcriptomic analysis of mouse retinal cells, demonstrated RFC1 mRNA in the pericytes, only if looked in detail [19]. As the prediction of protein levels by mRNA levels is considered imprecise [20], and does not automatically indicate the consistent presence of RFC1 protein or its functionality, the functional presence of RFC1 protein in the inner BRB or retinal pericytes is an unanswered scientific question. Therefore, considering the morphological and functional resemblance of the inner BRB and BBB, our first aim was to study if RFC1 protein is present in the endothelial cells and pericytes of inner BRB akin to their existence in BBB.

Cerebral and retinal ischemia can be considered comparable due to their similar microcirculation characteristics in both systems. Retina is particularly suited to diseases involving ischemia owing to its high metabolic rate necessitating constant blood supply via specialized capillary network [3, 4, 21, 22]. In the RPE, RFC1 expression and activity have been shown to vary during oxidative stress, hyperglycemia, nitric oxide exposure, and hyperhomocysteinemia [14, 15, 17], implying the potential role of RFC1 in pathologic states like ischemia. On the other hand, human studies demonstrated that RFC1 single nucleotide polymorphisms (SNPs) were related to ischemic stroke especially from the perspective of small vessel occlusions and silent brain infarctions [23]. However, the function of RFC1, expressed extensively in the brain endothelial cells of BBB, has not been investigated in the pathophysiology of ischemia or stroke but rather been studied in the hope of utilizing it as an alternative folate transport pathway to the brain in neurometabolic disorders in which cerebral folate delivery via choroid plexus is compromised. While choroid plexus harboring the other folate transport systems (i.e. folate receptor alpha [FRα; FOLR1], proton-coupled folate transporter [PCFT]) is mainly the responsible entity for folate delivery to brain parenchyma via transcytosis and exosome shuttling, BBB is determined to be the second major route since it provides ideal physiological conditions for transporting 5-methyltetrahydrofolate, major circulating form of folate, via abundant RFC1 expression [24]. Several studies which were concentrated on the regulation of RFC1 in the BBB *in vitro, ex vivo*

or *in vivo* have recently illuminated that RFC1 expression is actively controlled in BBB via transcription factor receptor of vitamin D or nuclear respiratory factor-1 (NRF-1) which binds RFC1 promoter [12, 25]. The transport characteristics of RFC1 has been studied in several cell lines as it transports antifolates (i.e., folate antagonists) such as Methotrexate (MTX) which are widely used as antineoplastic and antirheumatic agents in human [26, 27]. Recent findings have highlighted a novel role of RFC1, other than carrying folates or antifolates, in antiviral and antitumoral response as an importer of immunotransmitters, such as cGAMP and other cyclic dinucleotides [28, 29]. These suggest that its function might not be only limited to folate transport. Considering that RFC1 is one of the most consistently expressed gene in pericytes -the cells that play a key role during retinal and cerebral ischemia-, our second aim was to evaluate the role of RFC1 during retinal ischemia, both from the physiological perspective and as a novel therapeutic target in this common condition with a poor prognosis.

Here, after characterizing RFC1 in retinal microvessels, we attempted to provide initial proof of concept by modifying RFC1 *in vivo* in the retina to discover the role of RFC1 protein in the inner BRB in healthy and ischemic states. We employed a custom-designed RFC1-targeted Accell short interfering RNA (siRNA) to silence the RFC1 gene, and a lentiviral vector to overexpress RFC1 in the naive retina *in vivo*. As a pharmacological intervention, we intravitreally administered a single dose of MTX, which is a competitive inhibitor of folate transport via RFC1. Thus, we identified RFC1 as having the utmost importance in maintaining inner BRB both in health and retinal ischemia.

METHODS

Animals

Experiments were performed according to the approval provided by Hacettepe University Animal Experimentations Local Ethics Board (No: 2019/13-06 and 2021/03-19). Adult female and male Swiss albino mice (25–35 g) housed under 12 hours of light and 12 hours of darkness at standard room temperature (22±2°C) and 50-60% humidity were used for *in vivo* experiments. Mice were allowed to water and food ad libitum. The recommendations of ARRIVE guidelines and institutional instructions were taken into account in housing, care, and while performing experiments, the experimental groups were decided in a randomized and blinded manner. For all the surgical procedures mentioned below, the animals were anesthetized with ketamine (80 mg/kg, intraperitoneal injection, Ketalar®, Pfizer, Cambridge, United Kingdom) and xylazine (8mg/kg, intraperitoneal injection, Alfazyne® 2%, Alfasan International, Woerden, the Netherlands). A rectal probe connected to the homeothermic blanket with a control unit (Harvard Apparatus, U.S.A.) was utilized to control the body temperature (37.0±0.5°C). Pulse rate and oxygen saturation were monitored from the right lower limb monitored via an oximeter (The LifeSense® VET Pulse Oximeter, Nonin Medical Inc., USA). Vital signs (rectal temperature, blood pressure, oxygen saturation, and pulse rate) were kept within physiological limits and recorded. After operations, mice were put on homoeothermic blanket until they recovered from anesthesia fully. Next, the mice were kept individually in their cages until sacrificed.

Retinal Ischemia Model

The retinal ischemia model used here was previously developed in our laboratory and explained in detail elsewhere [30]. In short, anesthetized mice were put in prone position under a stereoscope (SMZ1000, Nikon Instruments Inc., Amsterdam, The Netherlands) and their heads were immobilized with a nosepiece. Central retinal artery located in central optic nerve were exposed via cautious retroorbital dissection. A small strip (0.3 × 1 mm) of 30% $FeCl_3$–soaked filter paper was placed on the optic nerve for 3 min to trigger clot formation and occlude central retinal artery. Regional retinal blood flow was monitored via Laser speckle contrast imaging (LSCI) to confirm ischemia as detailed [22].

Based on our previous observations, we used 1 hr of ischemia, as it was sufficient to induce ischemic changes in the microcirculation such as mural cell contractions [4, 22]. One hr later, eyeballs were collected under anesthesia, and animals were sacrificed by cervical dislocation.

Laser Speckle Contrast Imaging (LSCI)

LSCI was applied to confirm regional retinal blood flow drop and verify ischemia [22]. The pupils were dilated with 1% tropicamide (Bilim İlaç, Istanbul, Turkey) and a video camera with a charged-coupled device (CCD) (Basler 602F, Basler Vision Technologies, Germany) was installed 10-12 cm above the eyeball of the prone positioned mice. Thereafter a lens (Ocular Instruments, Bellevue, WA) was placed on the eyeball, which was illuminated by a power laser diode (785 nm, < 10mW) aimed at the retina with the help of a stereomicroscope (SMZ1000, Nikon Instruments Inc.). Ten baseline speckle images at 100 Hz at 10-second intervals were acquired and, processed by calculating the speckle contrast with a boxcar average of 7 × 7 pixels and averaged to enhance the signal-to-noise ratio. The images of relative blood flow (RBF) images were computed by calculating the flows of pre-ischemic and post-ischemic conditions leading to pseudo-colored images. Data was calculated relative to the baseline which was considered as zero-flow [22].

Intravitreal Methotrexate (MTX) Injection

For all intravitreal injections, mice were anesthetized with ketamine/xylazine, placed on a homeothermic blanket under a surgical microscope [31], and stabilized with a nosepiece which allows free neck movements to align the vitreous cavity and fundus under the objective. After dropping lubricant (Allergan, Inc. Irvine, CA 92612, USA) on the cornea, it was covered with a glass coverslip. This served as a mean to visualize the needle tip during the intravitreal injection. Methotrexate (MTX) (1 µl of 50mg/5ml solution; Koçak Farma, Turkey) was delivered via 33 G Neuros Syringe (1701 RN, Hamilton) through the puncture at a 45° angle into the vitreous cavity [32]. Animals that developed opacification in lenses indicating redundant effects like vitreous hemorrhage or local infection were excluded. One hour after the injection, eyeballs were collected. As controls, animals were administered with the equal volume of vehicle which was sterile water.

Gene Silencing *In Vivo* by Short Interfering RNA (siRNA)

To silence RFC1 gene, we used two custom-designed mouse RFC1 (Slc19a1) Accell siRNAs targeted to two different regions of RFC1 mRNA and two Accell scrambled (control) siRNAs (Horizon Discovery, Waterbeach, United Kingdom). Accell siRNA has several advantages as it does not need any transfection reagents which may have unwanted effects when applied *in vivo*. Furthermore, they could be internalized by any type of mammalian cells [33] Accell siRNAs have been previously proven to be uniformly distributed across rat retinal tissue and successfully inhibit various genes following intravitreal delivery [34]. Product codes of siRNAs with sequences are given in Table 1. RFC1-siRNA-1 and RFC1-siRNA-2 or scrambled (control) siRNA-1 and 2 were pooled in equal volumes for administration to improve the potency and specificity.

	Product codes	**Sequences of sense strand**
RFC1-siRNA-1	A-044248-13	C.C.A.G.C.C.U.A.C.U.U.C.A.U.G.C.U.U.U.U.U
RFC1-siRNA-2	A-044248-15	C.C.A.G.G.A.A.A.C.U.A.G.A.U.C.G.C.A.U.U.U
Scrambled siRNA-1	D-001910-01	U.G.G.U.U.U.A.C.A.U.G.U.C.G.A.C.U.A.A.U.U
Scrambled siRNA-2	D-001910-03	U.G.G.U.U.U.A.C.A.U.G.U.U.U.U.C.C.U.A.U.U

Table 1. The product codes and the sequences of sense strands of RFC1-siRNAs and scrambled (control) siRNAs.

The injected solution containing siRNA were made according to the manufacturer's guidelines. In short, lyophilized siRNA was reconstituted in sterile RNase-free water (10977-035, Invitrogen™). Ultraviolet (UV) wavelength range spectrophotometer was used to determine the concentration of

siRNA. The final concentration of 100 µM for each siRNA stock solution was aimed. To prevent freezing and thawing cycles, stock solution was aliquoted into smaller volumes to be stored at -20°C. Individual stock solutions of RFC1-siRNAs and scrambled siRNAs were pooled in equal volumes on the day of injection.

We delivered RFC1-siRNAs or Control-siRNAs intravitreally to eyes (2.3 µL/eye) of animals via 33 G Neuros Syringe (1701 RN, Hamilton). We did not utilize contralateral eyes as controls to avoid the possible transfer of siRNAs to the opposite side [35, 36]. After 24 hr, we either proceeded to retinal ischemia or sacrificed mice, and determined the levels of mRNA or protein.

Quantitative Reverse Transcriptase-Polymerase Chain Reaction (qRT-PCR)

Eyeballs were freshly dissected in ice-cold sterile PBS under a surgical microscope to get the retina intact. The RNA from whole retinas was extracted via TRIzol Reagent (Invitrogen) according to the manufacturer's guidelines. The retinal RNA was then reverse transcribed to cDNA with a high-capacity reverse transcription cDNA kit (Applied Biosystems). Primer pairs specific to mouse RFC1/SLC19a1 (Mm00446220_m1) and Tubb4a (Mm00726185_s1, beta 4A class IVA as a housekeeping gene) were constructed and verified by Life Technologies to use with TaqMan qPCR chemistry (TaqMan™ Gene Expression Assay, Applied Biosystems™, 4331182). Briefly, the assay contained a couple of unlabeled PCR primers and a 5' dye-labeled TaqMan probe (FAM) and a 3' minor groove binder (MGB) and non-fluorescent quencher (NFQ). Amplicon context sequences for SLC19a1 and beta 4A class IVA are shown in Table 2. Using these assays, qRT-PCR analysis was performed to calculate the relative fold change in mRNA expression level of the SLC19a1 after siRNA administration. The critical threshold cycle (CT) of SLC19a1 gene was first normalized to the beta-tubulin 4A with the comparative CT method. The ΔCT which is the difference in CT values between the SLC19a1 and beta-tubulin 4A genes were then normalized to the corresponding ΔCT of the control siRNA group, expressed as ΔΔCT and calculated as fold change ($2^{-\Delta\Delta CT}$).

Symbols	**The full names of genes**	**Accession numbers of transcripts**	**Amplicon context sequences**
RFC1/SLC19a1	Mus musculus solute carrier family 19 (folate transporter), member 1 [Mus musculus (house mouse)]	NM_031196.3:1240-1390	CGGGACATCTGGGTG TGCTACGTGACCTTT GTGCTTTTCCGTGGG GCCTACCAGTTCCTT GTGCCCATTGCCACT TTTCAGATTGCGTCTT CCCTGTCTAAAGAGC TCTGTGCATTGGTCTT TGGGATCAACACTTT CCTAGCTACTGCGC
Tubb4a	Mus musculus tubulin, beta 4A class IVA (Tubb4a)	NM_009451.3:1852-2030	CCACCTTCTTAGATCT TGAAAATCCTTTCCTT TATGCCCTGTCCCTTC CCCAGCACTCCTGAA CCATTCTCCTCCACCT CTGACATGCCCAGAT ATTTCTCTAGATCTTA ACATTTTCCCCAGCC TCCAAGTCCTCTCAC CTTGCCTTACCTCTGA CCTCACAGCTACCCA CTCCTGAC

Table 2. Gene symbols, the full names of the genes, accession number of transcripts and amplicon context sequences of SLC19a1 and beta 4A class IVA.

Gene Overexpression *In Vivo* by Lentiviral Vector (LV)

Lentiviral vectors (LV) that express either green fluorescent protein (GFP) (Control-LV) or GFP with RFC1 (RFC1-LV) driven by EF-1 alpha promoter were used to overexpress RFC1 gene in the retina.

Cloning of RFC1-LV or Control-LV

The lentiviral packaging system used was second-generation, which was an effective and safe technique in producing LV. Total RNA from cultured mouse neuro 2a cell was extracted using AllPrep DNA/RNA/Protein Mini Kit (80004, Qiagen, Hilden, Germany) following the manufacturer's instructions. Transcriptor First Strand cDNA Synthesis Kit (04896866001, Roche, Basel, Switzerland) was used to obtain complementary DNA (cDNA). The coding region of mus musculus SCL19a1 variant 1/RFC1 (NCBI Reference Sequence: NM_031196.3) was amplified with specific primers (forward 5'-agtcagaattcatggtgcccactggccag-3'and reverse 5'-AGTCAGGATCCTCAAGCCTTGGCTTCGACTCTT -3') with fast digest restriction enzymes EcoRl (FD0274, Thermo Fisher Scientific, Massachusetts, USA) and BamHI (FD0054, Thermo Fisher Scientific). Restriction enzymes BamHI and EcoRI were used to digest the PCR product of SLC19a1 and expression plasmids (pLenti-EF1α-GFP-2A-Puro; Applied Biological Materials, Richmond, Canada). Subsequently, ligation was realized with T4 DNA ligase (EL0014, Thermo Fisher Scientific). Sequencing pMD2.G and psPAX plasmids, kindly provided by Dr. Didier Trono (Ecole Polytechnique Federale, Lausanne, Switzerland), were used to confirm the insert. They were employed as complementary vectors of the packaging of the lentiviral system (12259; 12260, Addgene, United Kingdom). HEK293T cell line (6×10^6 cells) was chosen to be seeded on 10 cm plates (CLS3294, Corning, New York, USA). The following day, the vector transfection Lipofectamine 3000 (L3000015, Thermo Fisher Scientific) was applied according to the manufacturer's instructions. Shortly, 7 μg lentiviral vector, 3.5 μg pMD2.G, and 7 μg psPAX were used to prepare DNA-lipid complex. The DNA-lipid complex was added slowly after 10 min of incubation at room temperature. Six hours after transfection, the medium was changed with fresh DMEM (P04–01158, Pan Biotech, Bavaria Germany) and was incubated at 37°C in a humid atmosphere consisting of 5% CO_2. Twenty four and fifty two hours following the transfection, the medium was harvested, centrifuged (10 min at 2000 rpm), and filtered with a low binding filter with a 0.45 μm pore size. After ultra-centrifuging (120,000 g for 2 hr), viral particles were dissolved in Dulbecco's Phosphate Buffered Saline (PBS) without calcium and magnesium (P04–3650, Pan Biotech). The plasmid with no DNA inserted was packaged with the same procedures to use as a control. The viral titer (1×10^8 lentivirus particles in 1 μl 0.1 M PBS) was measured by a previously published protocol [37].

LV (1×10^8 lentivirus particles in 1 μl 0.1 M PBS) were intravitreally delivered to the retina (2 μL/eye) via 33 G Neuros Syringe (1701 RN, Hamilton). Ten days after the delivery, we either proceeded to retinal ischemia or sacrificed mice to obtain eyeballs.

Retinal Whole Mount Preparation

The eyeballs harvested were immersed in 4% paraformaldehyde (PFA) for 1 hr, and under a stereo microscope, we made a puncture at the corneal border with an insulin needle while eyeballs were resting in one drop of PBS at room temperature. A circular cut along the limbus was made with the help of a micro-dissector. Following the extraction of the lens and vitreous body, the intact retina was detached from the sclera via a 45° thick curved tip tweezer by going around the edges. The retina was cut in each quarter like a clover with a micro-dissector to flatten it out. Then, the flattened retina was placed into a centrifuge tube consisting of 200 μL PBS for immunohistochemistry.

Retinal Trypsin Digest Preparation

We used modified retinal trypsin digestion protocol to isolate retinal microvessels from the surrounding tissue [38, 39]. Retinas were separated in cold Phosphate Buffered Saline (PBS), then immersed in 250 µL filtered ddH_20, and, at room temperature, kept on a shaker until they were disintegrated. Then kept in 0.3% trypsin (PAN Biotech 1:250) 0.1 M Tris buffer (pH 7.8) in the incubator adjusted to 37°C. The separation of microvessels from retinal tissue was checked under a microscope every 5 minutes. When microvessels were seen clearly, tissue was washed with dH_2O, and the procedure was repeated until no debris remained. Isolated retinal microvessels were transferred to poly-L-lysine coated slides with pipettes with trypsinized tips, without disrupting their integrity, and air-dried. This method allowed isolation of the retinal vessels containing endothelial cells, basal lamina, pericytes, the attached perivascular astrocyte processes [38], without the presence of other cell types like photoreceptor cells.

Immunohistochemical Studies

For immunohistochemical studies whole mount retinas, coronal sections and isolated retinal vessels were used. PFA fixed whole mount retinas were kept in in 0.5% PBS-Triton-X, freezed 15 min at -80°C and thawed for 15 min at room temperature following overnight incubation in 2% TritonX-100 (Merck Millipore, 1086031000) PBS for permeabilization. They were immersed in 10% normal goat serum for blocking step for 2 hr at room temperature or overnight at +4°C. Next, whole mount retinas were incubated at 4°C with primary antibodies against RFC1 (SLC19a1, MyBioSource MBS9134642 or Sigma-Aldrich AV44167) for three consecutive overnights. We used two commercial polyclonal antibodies developed against different non-overlapping epitopes of RFC1. RFC1/SLC19a1 antibody from MyBioSource (MBS9134642) was produced against a recombinant fusion protein containing a sequence related to amino acids 452-591 of human SLC19A1 (NP_919231.1), while RFC1/SLC19a1antibody from Sigma-Aldrich (AV44167) was produced against Synthetic peptide directed towards the N terminal region of human SLC19A1 (NP_919231). Then retinas were subsequently incubated with 'Fluorescein' or 'Texas Red' labeled Lectin (Vector Laboratories, Burlingame, CA). Following the permeabilization step with 0.3% TBS-Triton-X for 30 min, retinal microvessels obtained via retinal trypsin digestion were blocked in 10% normal serum of the host of the associated secondary antibody for 1 hr at room temperature. Vessel webs were incubated at +4°C overnight with primary antibodies against RFC1; for mural cells against PDGFR-β (R&D Systems, AF1042), NG2 (Sigma AB5320A4), CD13 (Acris Antibodies, AM26636AF-N), for endothelium CD31 (BD Bioscience, 550274); for tight junctions ZO-1 (Sigma, MAB1520), Claudin-5 (Invitrogen™, 35-2500), and for Collagen-4 (Abcam, ab6586) (n=3-6/marker). After several washes, the vessel webs were incubated for 1 hr at room temperature with appropriate Cy2-, Cy3- or Cy5-conjugated anti-rabbit IgG (Jackson ImmunoResearch 111-165-144 or 711-175-152) or anti-rat IgG (Thermo Scientific™, A10522, 1:200). To assess the inner BRB integrity, PFA fixed whole mount retinas were incubated with Cy3-conjugated anti-mouse IgG (Jackson ImmunoResearch, 115-165-003) at +4°C overnight. Later, retinas were incubated with 'Fluorescein' or 'Texas Red' labeled Lectin (Vector Laboratories, Burlingame, CA) at +4°C overnight to visualize the vessels. Washed with TBS for 3 times, 5 min each; retinal tissues or retinal microvessels were mounted with a PBS/Glycerol mounting medium consisting of the nuclear staining Hoechst 33258 (Invitrogen™, 1:1000 dilution).

Western Blotting

Whole retinas were lysed in Radioimmunoprecipitation assay (RIPA) buffer, sonicated, and homogenized on ice, then centrifugated at 10,000xg at +4°C for 20 min. The concentration of the lysates was assessed using BCA protein assay kit (Thermo Scientific™, 23225). After loading proteins (35 µg/well) to a homemade SDS-PAGE gel, 120 Voltage were applied for 1.5 hr. Proteins were then transferred to PVDF membranes by applying 120 mAmp/membrane for 2 hr at room temperature. Membranes were incubated with 5% BSA in 0.1% TBS-Tween for 1 hr at room temperature for blocking step, and incubated with 1:1000 anti-RFC1 antibody produced in rabbit (Sigma-Aldrich;

AV44167) at +4°C overnight. After washing with 0.1% TBS-Tween, we incubated the membranes with 1:5000 goat anti-rabbit HRP conjugated Invitrogen™, 31460) solution for 2 hr at room temperature. For detection, the membranes were treated with a high sensitivity enhanced chemiluminescent (ECL) substrate (Thermo Scientific™, 34096). Imaging was done by Kodak 4000M Image Station. Beta-tubulin III (Chemicon, MAB1637) was used as an internal standard for retinal ex-vivo tissue lysates obtained from animals. β-Actin and β-tubulin III was employed as an internal standard for cell culture homogenates and tissue homogenates respectively. Densitometric measurements were done by ImageJ 1.52 version (NIH, Bethesda, Maryland), and expressed as ratios to the internal standard.

Imaging and Analysis

The images of the stained whole mount retinas and retinal microvessels were obtained with a Leica TCS SP8 confocal laser scanning microscope (Leica, Wetzlar, Germany) with a diode laser 405, 638 and OPSL 488, 552 nm, with a X, Y, and Z-movement controller, and a high-resolution PMT (Zeiss, Oberkochen, Germany) and HyD (Leica) detectors. Images were either acquired in single focal plane while keeping settings constant between experimental or control groups for analysis or Z-stack mode with 0.80 µm wide steps along the Z axis. For analysis of immunostained retinal microvessels, 1024x1024 pixels and 276.79x276.79 µm sized, middle of the Z axis level images were used. Acquired images were exported as 8-bit grayscale .tiff formats from Leica Application Suite X (LAS X; version 3.5.5.19976) and opened in ImageJ 1.52 version. First, the lectin frame of each image was filtered by Gaussian blur (sigma=4) to reduce the random noise, and Huang Thresholding was applied to mask the lectin-positive microvessel areas of the images. After de-speckling (Process tab>Noise>Despeckle) and eroding (Process tab>Binary>Erode), the binary image was divided by 255 using Math function (Process tab>Math>Divide) to convert microvessel pixels to "1" and background pixels to "0". Later, either "RAW" lectin image or the overlapping grayscale image belonging to tight junctions or collagen-4 was divided by the lectin image binary. This created 32-bit grayscale images in which microvessels had singular intensity and the background had infinity. Finally, the mean grey value (RFU, range between 0-255) was obtained which corresponded to the mean intensity of the pixels occupying the microvessel area (Supplemental Fig. 1). Number of pericytes were quantified from Lectin and Hoechst labelled microvessel preparations by researchers blinded to the experimental or control groups. As pericytes are well known to have protruding nucleus, they were easy to distinguish morphological and spatially from endothelial cells having flat nucleus. The total microvessel length was measured with AngioTool (v 0.6a (64 bits), October 2014) software, and pericyte number per millimeter (mm) of microvessel length was calculated [40].

Statistical Analyses

All in vivo experiments were repeated in at least n=3 mice/group including the same amount of female and male mice. The number of mice per group for *in vivo* experiments are mentioned in the figure legends. All results were conveyed as mean ± standard error of the mean (S.E.M.). Data were analyzed using IBM SPSS 23. Non-normally distributed data were compared using the Mann-Whitney U test (for two groups). The expression ratio in a treatment group was expressed as a percentage of the ratio in the control group. $p \leq 0.05$ was considered significant.

RESULTS

RFC1 protein is abundantly expressed in the endothelial cells and pericytes of retinal microvessels

We isolated retinal microvessels by trypsin digestion technique which allowed us to study merely and in great detail the microvessels consisting of endothelial cells sealed by tight junctions, enclosed by basal lamina, and pericytes; concurrently, preventing the view to be disguised by parenchymal cells

[38], and to observe the colocalization of RFC1 protein specifically in the cells of our interest. We observed that RFC1 immunoreactivity was distributed continuously and diffusely throughout the retinal microvessels (Fig. 1A), and colocalized with fluorescently labeled lectin which stereospecifically binds to glycocalyx layer covering the endothelial cells (Fig. 1B). RFC1 was immunohistochemically co-labeled with the endothelial marker, cluster of differentiation 31 (CD31), whose immunoreactivity exclusively outlined the endothelial cells. As a convincing finding that there was no crosstalk in immunoreactivity, RFC1 labeling was determined to localize to both the endothelial cells, and to the 'bump on a log' shaped cells (Fig. 1C, arrows), which classically is suggestive of pericytes.

We then labeled the microvessels with well-defined pericyte markers including the neural/glial antigen 2 (NG2), platelet-derived growth factor receptor beta (PDGFR-β), and aminopeptidase-N (CD13), all of which showed a strong colocalization with RFC1 (n=3-5 retina per marker, Fig. 1D-F). These indicated that RFC1 was present both in the endothelial cells and pericytes.

Our internal positive control was the retinal pigmented epithelium (RPE) that is known to be immunohistochemically positive for RFC1 [41] (Fig. 1C). Besides RPE, the coronal retina sections displayed RFC1 immunoreactivity at the other layers of the retina, and was particularly strong in the ganglion cell layer, inner and outer plexiform layers (Supplemental Fig. 2A) that coincided with the superficial and deep microvascular plexus, the two-layered interconnected plexus of vessels arising from the retinal arterioles. Hence, the immunosignal was detected in the retinal layers with microvessels. We also used whole mount retina preparations that required a longer incubation period with a higher concentration of anti-RFC1 antibody when compared to isolated microvessel immunohistochemistry and determined RFC1 (Supplemental Fig. 2B) positive microvessels forming deep plexus.

Since either homemade antibodies or RFC1 antiserum was used for immunohistochemistry of various organs and organisms previously [10, 29, 42], we employed two different currently available commercial antibodies bearing different features [MyBioSource (MBS9134642); Sigma-Aldrich (AV44167)]. We also used the kidney, choroid plexus, and small intestine which had zones with and without RFC1 expression as positive and negative tissue controls [43]. We observed RFC1 immunostaining at the kidney proximal tubules in mice where folate reabsorption occurs (Supplemental Fig 2C, arrows), yet kidney glomeruli, which are formed by specialized microvessels with fenestrated endothelial cells with no RFC1 served as a negative tissue control (Supplemental Fig 2C, asterisk). Choroid plexus ependymal cells and small intestine epithelia (Supplemental Fig. 2D, E respectively) were other tissues in which RFC1 expression was estimated and observed. Overall, these data provided support for the specificity of the antibody in our study to detect RFC1 immunoreactivity in retinal endothelial cells and pericytes.

Retinal RFC1 is downregulated *in vivo* by RFC1 targeted Accell siRNA, and leads to disruption of the inner BRB

We delivered a combination containing the same amount of specifically designed two RFC1 targeted Accell siRNAs (RFC1-siRNA) or two scrambled siRNAs intravitreally and sacrificed the mice 24 hr later (Fig. 2A). To confirm the knockdown of RFC1, we obtained fresh whole retinas and determined the change in RFC1 mRNA expression by qRT-PCR. RFC1-siRNA significantly decreased RFC1 mRNA by 24.75% compared to scrambled siRNA (p= 0.004, Supplemental Fig. 3A). We also confirmed the reduction via Western Blotting (Supplemental Fig. 3B) and determined pronounced decrease of RFC1 protein. In line with these, RFC1 immunosignal intensity was less in the microvessels of RFC1-siRNA injected retinas (72.1%, $p<0.0001$; Fig. 2C, D). We also noticed that RFC1-siRNA treated retinas were fragile, and prone to damage during the procedures.

As we determined that retinal microvessels express RFC1 protein abundantly, and we could efficiently knock down RFC1 *in vivo*, we elucidated whether RFC1 suppression may lead to any changes in the inner BRB.

Strikingly, knocking down retinal RFC1 diminished immunoreactivity of the tight junction-associated transmembrane proteins occludin, claudin-5, and cytoplasmic adaptor protein zonula occludens-1 (ZO-1), as well as the main basement membrane protein collagen-4 in trypsin digested microvessels (n=3 retina/per marker, Fig. 2E-H). In RFC1-siRNA treated microvessels, immunoreactivity of collagen-4 that surrounds the abluminal membrane of endothelial cells and covers pericytes residing in the basement membrane decreased by 68% (p=0.0043), occludin decreased by 57.03% (p=0.0043), and claudin-5 decreased by 76.26% (*p*= 0.0006). ZO-1, the intracellular adaptor protein establishing a link between occludin and intracellular actin cytoskeleton decreased by 53.22% (p= 0.0012).

The immunostaining of the whole mount retinas also confirmed RFC1-siRNA knockdown with diminished RFC1 immunosignal, and further showed that Lectin stainings (Fig. 2F, I, J) were weaker and interrupted in RFC1-siRNA treated preparations, indicating that microvessels might be structurally damaged. In addition, these retinal microvessels demonstrated lower NG2 signal compared to scrambled siRNA treated ones, which suggested that pericytes might also be damaged by RFC1-siRNA (Fig. 2K, L). However, to address if the reduction in RFC1 immunoreactivity in siRNA treated microvessels might be associated with the loss of pericytes, we assessed pericyte density (soma per millimeter capillary). We found no significant decline in pericyte density in RFC1-siRNA administered retinas suggesting that RFC1 decrease may not affect pericyte maintenance, as it did not reduce pericytes in number at least at this early timepoint (Fig. 2M). However, we could not exclude disruption of pericyte functions via RFC1-siRNA, since there is marked decline in the expression of pericyte marker NG2, and the deterioration of tight junction proteins and collagen-4.

RFC1 knockdown resulted in the disruption of inner BRB, and is determined by increased endogenous IgG extravasation. Whole mount retinas from RFC1-siRNA treated mice were stained with lectin and a fluorescently labeled anti-mouse IgG antibody to label endogenous IgG, which showed endogenous IgG extravasation (Fig. 5B, red arrows), while scrambled-siRNA treated retinas did not show any (Fig. 5A). This indicated that RFC1 is essentially required for the functional maintenance of the inner BRB in health.

Retinal RFC1 is upregulated *in vivo* by LV overexpressing RFC1, and this upregulation changes the inner BRB properties

Next, we aimed to increase the expression of RFC1 in naive mouse retinas via LV carrying RFC1 as described in detail in the methods section and shown in Supplemental Fig. 4A. We preferred the LV gene delivery method due to its efficiency to induce stable gene expression, its tropism to the inner retina and the cells surrounding or constituting retinal microvessels when delivered intravitreally [44, 45].

Control-LV or RFC1-LV vectors were tested in vitro by visualizing green fluorescent protein (GFP) in a transduced neuroblastoma cell line (N2a) (Supplemental Fig. 4B), and the efficient RFC1 protein overexpression was shown by Western Blotting (Supplemental Fig. 4C). Subsequently, we proceeded to validate the LV-mediated transduction *in vivo*. Mice were intravitreally delivered unilaterally. There were no animals developing any local infection after lentiviral vector injection for 10 days. The eyeballs of three mice that received intravitreal Control-LV injection were harvested under anesthesia 10 days after the procedure to dissect and prepare either whole mount retinas or retinal trypsin digest preparations. In the whole mounts, the retinal layers and microvessels were imaged by confocal laser scanning microscopy showing extensive GFP expression localized in perivascular cells and pericytes (Supplemental Fig. 4E, F). As expected, no GFP expression was observed in the non-injected control

retinas which were obtained from animals not administered lentiviral vectors and euthanized under the same conditions (Supplemental Fig. 4G).

The overexpression of RFC1 by LV delivery in the retina was validated by immunofluorescence in the whole mount retinas and retinal microvessels obtained via retinal trypsin digestion (Fig 3A). RFC1 immunoreactivity revealed a marked increase in intensity in both the retinal whole mounts (Supplemental Fig. 4H, I) and retinal microvessels compared to controls (Fig. 3C-D). Retinal microvessels of RFC1-LV administered mice showed 167.5% increase in RFC1 immunosignal compared to Control-LV administered ones (p= 0.0159).

As pharmacological interventions are a common approach to determine the effects of changes in protein levels or functions; MTX, which is the substrate of RFC1, and a competitive antagonist of folate was used to observe its potential effect on RFC1. A single dose of MTX was delivered intravitreally. Mice were sacrificed 1 hr later and their eyes were enucleated to obtain whole retinas or to isolate microvessels. We observed RFC1 immunoreactivity increase in a punctate pattern in retinal microvessels compared to vehicle-injected controls (p=0.0427). Also, in microvascular segments which were focally contracted underneath the pericyte bodies, a further increase in RFC1 immunoreactivity was noted (white arrows, Supplemental Fig. 4B, D). To assess RFC1 protein levels in retinas, we performed Western Blotting from intravitreally MTX-injected animals and vehicle injected controls. We observed an increase in the relative band density of RFC1; however, this change was not significant statistically (p>0.05) (Supplemental Fig. 5E, F), indicating that the increase in RFC1 level by MTX might solely be stemmed from retinal microvessels and not from other cells of the retina.

Keeping in mind that the suppression of RFC1 protein level by RFC1-siRNA had led to extensive structural damage in retinal microvessels and a decrease in immunoreactivity of tight junction proteins, we further investigated whether RFC1 overexpression via RFC1-LV administration had any effects. Immunohistochemistry was performed for tight junction proteins (occludin, claudin-5), intracellular adaptor protein ZO-1, and main basement membrane protein collagen-4 in isolated retinal microvessels (n=3 retina/per marker; Fig. 3E-H) ten days after administration of intravitreal Control-LV or RFC1-LV. As seen from quantified images of the RFC1-LV administered retinal microvessels, occludin (p= 0.0059), claudin-5 (p= 0.0040), and collagen-4 (p= 0.0159) immunoreactivity were increased by RFC1 overexpression in comparison to Control-LV administrated animals. However, the immunosignal of ZO-1 was not different between groups (Fig. 3B, E-H).

Retinal ischemia alters RFC1 protein and decreases retinal barrier proteins, which can be ameliorated by the overexpression of RFC1

After observing the potential role of RFC1 protein in maintaining inner BRB, we investigated whether RFC1 protein has any role in the pathophysiology of retinal ischemia. We applied 1 hr permanent retinal ischemia, as it is considered sufficient to observe microvessel-related changes such as capillary constrictions and outward protrusion of the contracted pericyte soma from microvessel wall, based on our previous observations yet this early timepoint allowed us to minimize the effects of inflammation [4, 21, 22]. Retinal ischemia was performed by $FeCl_3$ application as described in detail before [21] (Fig. 4A).

Ischemia-induced pericyte-mediated constrictions (Fig. 4D, yellow arrows) were present in the retinal microvessels. Discernible protruding segments in the bodies of pericytes were observed as the accustomed findings of ischemia (Fig. 4D, white arrows). Following ischemia, RFC1 immunoreactivity was augmented compared to controls and was found to be significantly increased when mean grey value of RFC1 immunosignal (i.e., fluorescence intensity) was measured (p <0.0001; Fig. 4C, D). Of note, the RFC1 signal was more pronounced in the protruding edge of pericytes (Fig.

4D, white asterisks). The relative expression of RFC1 was enhanced significantly compared to controls in Western blotting (p =0.025; Supplemental Fig. 5E, F).

We also studied whether 1 hr retinal ischemia caused any significant alterations in barrier proteins (n=3 retina/marker). We observed that 1 hr retinal ischemia decreased collagen-4 and occludin protein compared to control in the retinal microvessels (p =0.0140, p =0.0317 respectively; Fig4. E, F). We observed that 1 hr retinal ischemia did not significantly compromise the integrity of inner BRB (n=3; Fig. 5C). We then studied whether knocking-down RFC1 before ischemia may provoke disruption of the inner BRB. When RFC1-siRNA was administered 24 hr before retinal ischemia, we determined significant amount of endogenous IgG extravasation (Fig. 5D, red arrows), while scrambled siRNA administration 24 hr before retinal ischemia led no discernible IgG extravasation. This observation was significant since 1 hr ischemia only is such an early timepoint that it does not suffice for inner BRB opening to the extent of allowing leakage of endogenous IgG (150 kDa) through paracellular barrier even if disintegration of tight junctions had already commenced [46-48]. Thus, this indicated that decreased RFC1 levels may accelerate barrier disruption in retinal ischemia.

DISCUSSION

In this report, for the first time, we demonstrated the existence of RFC1 protein in the endothelial cells and pericytes of the inner BRB. Furthermore, we have shown that RFC1 - once an ignored transporter protein - is an essential component for maintaining the inner BRB and has fundamental roles in pathological conditions affecting inner BRB, such as retinal ischemia.

RFC1 expression at the protein level in endothelial cells and pericytes of retinal microvessels has never been studied before, despite its consistent detection in transcripts of microvascular mural cells (pericytes and vascular smooth muscle cells) of the brain [13]. The scarcity of antibodies for this transporter [29] until recently was a challenge for studies in this field; hence, most former studies used RFC1 antiserum or homemade antibodies to mark RFC1 protein in the tissues [10, 29, 42]. The availability of commercial RFC1 antibodies that were confirmed by immunohistochemistry in human, rat, and mouse (manufacturer information) and also by Western Blotting in Jurkat cell lines (manufacturer information) or in mouse brain capillaries [11, 12] facilitated the research in the field. In our study, we used two different antibodies and achieved successful negative and positive control immunostainings. We used high concentrations and long incubation durations like three overnights at +4°C with the primary antibody for the 200 µm thick whole mount retinal preparations to visualize retinal microvessels. Likewise, isolating retinal microvessels with the trypsin digestion method provided us with an easier and more consistent preparation for immunostainings. Our results highlight that retinal endothelial cells, similar to their counterparts in the brain, express RFC1 protein. As an additional novel finding we detected the colocalization of RFC1 with the well-defined pericyte markers. Most studies evaluating the role of RFC1 in microvessels concentrated on only the endothelial layer, but not the neighboring pericytes [10-12, 49]. In this regard, RFC1 protein was never characterized in central nervous system pericytes as well. Our findings actually match the results of a recent metanalysis combining five different mouse brain pericyte transcriptomic studies where the RFC1 gene was one of the only three consistently detected genes in brain pericytes out of the 1180 enriched genes [13].

Our study provides some initial insights regarding the functional importance of RFC1 in retinal microvessels. The genetic knockout of RFC1 is lethal [50] and no conditional knockout animals had been used in the studies before, so we decided to utilize siRNA technology to manipulate RFC1 levels specifically in the retina of adult mice. Two previous *in vitro* studies using RFC1-siRNA which were performed in primary cultures of human differentiated adipocytes [51], and in rat choroidal epithelial Z310 cells [24] did not focus on the microvessels or the retina. Hence, our method to knockdown RFC1 *in vivo* by RFC1 targeted custom designed Accell RFC1-siRNA could be considered as one of the initial efforts. RFC1-siRNA administration to the retina *in vivo* via intravitreal delivery offers

some advantages: 1) the retina is the easily reachable extension of the brain with a well-known anatomy 2) the vitreous cavity is an enclosed space that minimizes systemic spread and maximizes the applied concentration 3) delivery is fast and feasible [52]. The application of RFC1-siRNA deranged the structure of retinal microvessels, specifically the inner BRB, as shown by lectin stainings (Fig. 2J). Interestingly, knocking down RFC1 led to a significant decrease in the barrier proteins occludin, claudin-5, intracellular adaptor protein ZO-1, and the main basement membrane protein collagen-4. This induced inner BRB disintegration and led to functional failure of the barrier properties. Although it may be plausible to interpret this striking result with caution, there is a study showing that the tight junction proteins like occludin, claudin-1, and ZO-1 were substantially decreased in the BBB of capillaries isolated from proton coupled folate transporter (PCFT) null mice in comparison to controls [53]. However, this mouse with deleted PCFT gene - another functionally distinct folate transporter- is accepted as a model for hereditary folate malabsorption that leads to systemic folate deficiency. Hence, it is not possible to fully exclude the contribution of chronic folate deficiency to these effects. However, in our study, we observed inner BRB changes after acute modifications of the transporter in naive mice, which circumvents the confounding developmental effects of folate deficiency. In line with these observations, our experiments with the retinal overexpression of RFC1 via LV have shown an upregulation of occludin, claudin-5 and collagen-4, supporting the role of RFC1 in inner BRB protein expressions. As an interesting observation, RFC1 was recently determined as a cGAMP importer in the cyclic GMP–AMP synthase (cGAS)–stimulator of interferon genes (STING) pathway that has a role in inflammation, infection, cellular stress, tissue damage, and tumor angiogenesis [28, 29, 54]. In mouse tumor models, intratumoral cGAMP treatment led to a 40% decrease in the density of the vessels, a 1.7-fold rise in pericyte coverage, and a 1.5-fold rise in collagen-4 coverage [54], which may indicate that RFC1 may indirectly involve in remodeling the tumor vasculature in consistent with our observations in inner retinal microvasculature.

Based on reports that show pericytes are eminent for BBB and inner BRB maintenance and contribute to tight junction formation and preservation [55-58], we also excluded pericyte deficiency in RFC1-siRNA treated retinas. Although we found no significant decrease in pericyte density by counting pericyte soma per mm capillary in RFC1-siRNA treated mice, we observed immunosignal decrease in pericyte marker NG2, which involves in many functions of pericytes including proliferation, motility and importantly, endothelial cell junction assembly by activating integrin signaling [59]. For example, the treatment of human microvascular pericytes with NG2-siRNA hindered collagen-4 coverage, ZO-1 expression, and endothelial junction maintenance in endothelial monolayers. Likewise, in tumors from mice whose pericytes do not express NG2 showed similar changes in their endothelial junctions in the same study [60]. Although the underlying mechanisms require clarification, we suggest that NG2 might be a mediator of the effects observed in tight junction proteins and collagen-4 via RFC1-siRNA. Alternatively, the disintegration of NG2 in RFC1-siRNA treated retinal microvessels may indicate more comprehensive dysfunction throughout the inner BRB, to which NG2 disruption is only a contributing factor.

We also determined the effect of changes in RFC1 protein following pharmacologic manipulation with MTX. MTX, which is used clinically as an antineoplastic and antirheumatic agent, is a folic acid analog, and inhibits folic acid uptake acting as a non-covalent (competitive) inhibitor of RFC1. The failure of transportation of antifolates such as MTX, which inhibits enzymes participating in intracellular folate-dependent pathways crucial for cell proliferation also shown to be transported via RFC1, results in chemotherapeutic resistance [61]. Therefore, the transport characteristics of RFC1 are a well-studied field especially in vitro and tumor studies [27, 62, 63]. In wildtype ZR-75-1 breast cancer cell line, a single dose of 30 nM concentration of MTX administration caused 30% decrease in mRNA levels of RFC1 at 24 hours, and a decrease in RFC1 protein levels in the presence of 1 µM folic acid. [64]. We used intravitreal single dose MTX treatment for the pharmacological inhibition of RFC1 function, as we expected to block the function of the protein for a limited period of time, since

its intravitreal half-life was calculated to be 12.4-21.5 hr and systemic half-life was found to be 33.8±6.5 minutes in mice [32, 65]. Paradoxically, we observed an increased level of RFC1 in retinal microvessels following a single high dose of intravitreal MTX administration; yet the level of upregulation in RFC1 was less in comparison to the increase following LV treatment. Similar findings were also observed in prior studies after MTX administration, where the levels of dihydrofolate reductase protein which is another MTX substrate increased in studies of mammalian cells *in vitro* and *in vivo* [66-68]. In line with that, it was observed that MTX application in cisplatin-MTX sensitive leukemic cell line (L1210/0) increased the RFC1 immunosignal as early as 15 min after MTX incubation, however this upregulation was temporary, and RFC1 upregulation was reversed after 24 hr [69]. These findings suggest that MTX, competitive inhibitor of intracellular folate accumulation, may lead to acute upregulation of RFC1 by preventing the entrance of folate through RFC1. However, it should be noted that MTX has additional pharmacological outcomes including suppression of inflammation and interferes with many intracellular pathways and enzymes in folate cycle especially in chronic timepoints. Therefore, further research is needed to tease out the mechanisms and potential therapeutic role of MTX in this interplay.

Aside from its role in the maintenance of BRB under physiologic conditions, we further investigated the effect of RFC1 during retinal ischemia. Retinal ischemia which is a major underlying condition of blindness worldwide is a severe condition with a poor prognosis generally caused by acute occlusion of retinal arteries [70]. We induced retinal ischemia by an established method in our laboratory [22, 30], and showed an increase in RFC1 protein after 1 hr permanent ischemia. A previous gene profiling study, showed RFC1 mRNA upregulation following 1 hr ischemia / 24 hr recanalization induced by high intraocular pressure retinal ischemia model in rats [71]. In contrast, the same study observed no significant change in RFC1 mRNA in 1 hr permanent retinal ischemia. Another study showed that 45 min retinal ischemia followed by 48 hr recanalization upregulated RFC1 mRNA in rats [72]. The possible explanation for these results may be that the retinal ischemia models were different, and the authors only determined mRNA levels, not the protein levels of the samples. The estimation of protein levels from mRNA levels might be unreliable, as post-translational changes could affect the protein levels in early time-point [20]. There is only one study performed by kidney ischemia-reperfusion model that determined RFC1 protein levels decreased *in vivo* focusing on the proximal tubules where folate reabsorption occurs, emphasizing its importance in adjusting serum folate levels [73]. Contrarily, the increase of metabolic needs due to acute phase of ischemia might necessitate the upregulation of RFC1 after 1 hr of retinal ischemia for the preservation of the barrier properties. In line with that, further augmentation of RFC1 expression by LV-RFC1 intervention before ischemia salvaged the decreased occludin and collagen-4 levels, otherwise which would be attenuated by ischemia.

Also, knocking down RFC1 prior to ischemia impaired barrier functions which were demonstrated by endogenous IgG leakage, supporting our findings that RFC1 is essential for the protection of inner BRB during retinal ischemia. This result might be interpreted in the light of the human meta-analysis showing that the SNPs of RFC1 gene differed between ischemic stroke and control groups, and some genotypes were found to be associated with small vessel occlusions and silent brain infarctions [23]. Since the changes in RFC1 function or structure with these polymorphisms had not been defined, it is possible that our finding of changes in inner BRB via the genetical modifications of RFC1 could carry the potential of being the experimental evidence of the importance of RFC1 in ischemia and small vessel disease. Thus, intriguing questions regarding the therapeutic potential of intervening RFC1 before, during or after ischemia rises.

Limitations

Our study can be considered as an initial step to investigate the role of ‘once an unnoticed transporter protein’ in inner BRB. We took a step-by-step approach, defined the presence of the RFC1 protein in

the retinal microvasculature and made use *in vivo* tools to clarify potential new roles of RFC1 under physiologic conditions and ischemia. Some limitations of our study merit consideration. The genetic manipulations we used were not targeted specifically to endothelial cells or pericytes. We did not study the underlying mechanisms or pathways of how RFC1 regulates barrier proteins or BRB integrity. In addition, we have not performed measurements for the level of intracellular folate accumulation or studied how other BRB proteins affected by bidirectional manipulation of RFC1. Also, the interplay among other folate transport systems (FRα, RFC and PCFT) and the concert of the efflux systems (Pgp/ABCB1, MRPs/ABCC, BCRP/ABCG2) residing in inner BRB [74] to establish intracellular folate homeostasis was overlooked in this study, which warrants further investigations.

Implications

Despite these limitations, our data suggest several implications. We propose a conceptual model of workflow for the other proteins like RFC1 whose presence and roles have not been elucidated so far. Nowadays, the roles of these proteins have been investigated through advanced mathematical models, pathway analyses and the -omics approaches, but the old phrase "seeing is believing" should not be underestimated and *in vivo* studies may provide surprising insights into the role of a protein. The upregulation of RFC1 may be attempted for diseases other than ischemia where the impairment of BRB or BBB is involved in the pathophysiology. Although merely an initial step, our results are encouraging as the presence of RFC1 in inner BRB may be exploited for targeted drug delivery such as RFC1-targeted nanodrugs, folate conjugated nanodrugs or even MTX-coupled agents not only in ischemia, but in diseases like cancer.

Summary & Conclusion

In the present study, we investigated the presence of RFC1 in the retinal endothelial cells and pericytes, and its role in the regulation of inner BRB integrity. For the first time, we introduced and discussed the tools for the bidirectional manipulation of RFC1 levels or function *in vivo* which included RFC1-targeted Accell siRNA to knockdown RFC1, and LV to overexpress RFC1 as well as intravitreal MTX as a pharmacological agent. By using these tools, we tried to elucidate the role of RFC1 in the regulation of inner BRB during physiological conditions and ischemia and highlighted its potential role for preserving BRB integrity. This study aimed to precede the further investigation of RFC1 in other tissues and diseases by suggesting a conceptual and methodological framework. Future research may extend this work by integrating pathways which RFC1 is associated with to address the concern of how RFC1 regulated inner BRB.

Figure Legends

Fig 1. RFC1 protein is abundantly expressed in endothelial cells and pericytes of the retinal microvessels. A) Retinal microvessels which were obtained via retinal trypsin digestion method that allowed to get only microvessels (< 9 μm diameter) were immunofluorescently labeled with anti-RFC1 antibody (n=6 retina; red). Nuclei were labeled with Hoechst 33258 (blue) in all the rows. B) RFC1 (red) was colocalized with Fluorescein (FITC) labeled Lycopersicon esculentum (Tomato) Lectin (green) (n=3), which evenly labeled glycocalyx surrounding endothelial cells and pericytes, and C) the endothelial marker CD31 (green) (n=3). White arrow show "bump-on-a log" shaped pericyte body was positively stained with anti-RFC1 antibody, but negative for endothelial marker CD31. Hence, RFC1 staining was specific. D-F) RFC1 (red) also colocalized with accepted pericyte markers NG2, CD13, PDGFR-β (green) shown respectively (n=3/marker). Nuclei were labeled with Hoechst 33258 (blue). Scale bar: 10 μm.

Fig 2. Accell siRNA mediated *in vivo* RFC1 knockdown led to a reduction in proteins of the inner BRB. A) Schematic drawing of RFC1-siRNA delivery experiments. 100 μM siRNA was delivered intravitreally. After 24 hours animals were sacrificed, and retinas were collected for the analyses. B) The graphs illustrate the percentage of mean grey value of an image frame processed as described in Methods section. RFC1-siRNA delivery significantly reduced the percent of the mean grey values of RFC1 by 72.10% (n=4), Collagen-4 68% (n=4), Occludin 57.03% (n=3), Claudin-5 76.26% (n=4), and ZO-1 53.22% (n=4). The reductions that are statistically significant as represented as *$p \leq 0.05$, **$p \leq 0.01$, ***$p \leq 0.001$, ****$p \leq 0.0001$. C, D) Representative confocal images of Scrambled-siRNA or RFC1-siRNA delivered retinal microvessels stained by anti-RFC1 antibody (red). Noteworthy immunosignal decrease in RFC1-siRNA treated retinas were observed compared to Scrambled-siRNA delivered ones. E, F) Immunosignal decrease was also observed in collagen-4 (magenta), Occludin (cyan), Lectin (Yellow) as well as G, H) Claudin-5 (magenta), and ZO-1 (cyan) via RFC1-siRNA treatment compared to Scrambled-siRNA treatment. I, J) Whole mount retinas were labeled by anti-RFC1 antibody (red) and Fluorescein Lectin (green). RFC1 immunosignal was decreased and interrupted along deep retinal microvessels. Also, lectin signal was weakened in RFC1-siRNA treated retinas representing the structural decomposition of microvessels. K, L) Accordingly, RFC1-siRNA treated retinal microvessels showed less NG2 immunosignal compared to Scrambled-siRNA treated ones, indicating that pericytes might also be damaged by RFC1-siRNA. M) However, pericyte body counts per microvessel length (mm) were not different between the groups. n = 3 images were analyzed per animal; Nuclei are labelled with Hoechst 33258 (blue), Data are mean ± S.E.M Mann-Whitney U; Scale bar: 10 μm.

Fig. 3 Lentiviral vector-mediated overexpression of RFC1 protein *in vivo* resulted an increase in the proteins of BRB. A) Schematic drawing of the timeline of LV delivery experiments. 2 μL LV (1 x 10^8 lentivirus particles in 1 μl 0.1 M PBS) were delivered intravitreally. Animals were sacrificed after 10 days, and retinas were collected for the analysis (n=3). B) The graphs illustrate the percentage of mean grey value of a frame processed as described in Methods section. RFC1-LV delivery significantly increased the percent of the mean grey values of RFC1 (n=3), Collagen-4 (n=4), Occludin (n=3), Claudin-5 (n=3), but not ZO-1 compared to Control-LV delivered groups. *$p \leq 0.05$, **$p \leq 0.01$, ns: non-significant. C, D) Representative confocal images of Control-LV or RFC1-LV delivered retinal microvessels, immunohistochemically labelled by anti-RFC1 antibody (red). Significant immunosignal increase in RFC1-LV treated microvessels is observed compared to Control-LV delivered retinas. E, F) Collagen-4 (magenta), Occludin (cyan) Lectin (Yellow) immunosignal increased as well as G, H) Claudin-5 (magenta) except ZO-1 (cyan) via RFC1-LV treatment compared to Control-LV treatment. n = 3 images were analyzed per animal; Nuclei were labelled with Hoechst 33258 (blue) Data are mean ± S.E.M. Mann-Whitney U; Scale bar: 10 μm.

Fig 4. RFC1 protein increased after retinal ischemia, and the overexpression of RFC1 by LV decreased collagen-4 and occludin Levels. A) Schematic drawing of the timeline of retinal ischemia experiments and method. Permanent $FeCl_3$ retinal ischemia model which was performed by placing a small piece of (0.3 × 1 mm) filter paper saturated by 30% $FeCl_3$ for 3 min on optic nerve to occlude the central retinal artery. CRA: central retinal artery, LPCA: long posterior ciliary artery, ACA: anterior ciliary artery. B) The graphs illustrate the percentage of mean grey value of a frame processed as described in Methods section. Retinal ischemia significantly augmented the percentage of mean grey value of RFC1 by 114.5% (n=3). In contrast, it decreased collagen-4 by 42.07% (n=3), Occludin by 50.94% (n=3). In addition, microvessels treated with LV-RFC1, 10 days before ischemia showed 176% increase in Collagen-4 (n=3) and 60.9% in Occludin (n=3) compared to Control-LV delivered ones indicating RFC1 overexpression before ischemia might retrieve loss of collagen-4 and occludin in ischemia. *$p \leq 0.05$, ****$p \leq 0.0001$, ns: non-significant C, D) Representative confocal images of control or ischemic retinal microvessels stained by anti-RFC1 antibody (red). Significant immunosignal increase in ischemic microvessels was observed compared to controls. Also, ischemic microvessels demonstrated expected characteristics such as constrictions (yellow arrows) and protruding pericyte bodies (white arrows). Of note, ischemic pericyte bodies showed denser RFC1 immunosignal (white asterisks). Nuclei were labelled with Hoechst 33258 (blue) in all images. E, F) Collagen-4 (magenta) and Occludin (cyan) immunosignal was decreased with ischemia. G, H) LV-RFC1 delivery 10 days before ischemia salvaged Collagen-4 (magenta) and Occludin (cyan) levels as Control-LV delivered ischemic microvessels showed less Collagen-4 (magenta) and Occludin (cyan) immunosignal. n = 3 images were analyzed per animal; Data are mean ± S.E.M. Mann-Whitney U; Scale bar: 10 μm.

Figure 5. siRNA mediated RFC1 knockdown led to inner BRB breakdown and endogenous IgG extravasation. The wholemount retinas were labeled by Lectin (cyan) and incubated with Cy3 labeled goat anti-mouse antibody (yellow) to visualize the extravasated endogenous mouse IgG. A) RFC1-siRNA mediated knockdown led to significant IgG extravasation (red arrows) in microvessels while B) Control-siRNA treated retinas showed no extravascular IgG signal (n=3). C) 1 hr ischemia led to microvessel constrictions (white arrows) but no IgG extravasation. D) However, knocking down RFC1 before ischemia provoked inner BRB disruption leading to endogenous IgG extravasation (red arrows) (n=3). Nuclei were labelled with Hoechst 33258 (blue) in all images. Scale bar: 10 μm

ACKNOWLEDGMENTS

We thank Dr. Canan Cakir Aktas (The Institute of Neurological Sciences and Psychiatry, Hacettepe University, Ankara, Turkey) for assisting the financial management of the project, Dr. Buket Nebiye Demir (The Institute of Neurological Sciences and Psychiatry, Hacettepe University, Ankara, Turkey) for technical advice on in vivo procedures, and our laboratory technician Mesut Firat (The Institute of Neurological Sciences and Psychiatry, Hacettepe University, Ankara, Turkey) for providing technical assistance throughout project. We are grateful to our undergraduate researchers Derin Nalcakan and Neslihan Nisa Gecici (Hacettepe University Medical School), who were officially added as interns to the project with "TÜBİTAK-Intern Researcher Scholarship Programme", for their contribution to immunohistochemistry and data analysis. This research was supported by The Scientific and Technological Research Institution of Turkey (TÜBİTAK; Grant No: 120N690) and Hacettepe University Scientific Research Coordination Unit (Project No: TDK-2020-18590)

Abbreviations:

BBB: blood-brain barrier; BRB: blood-retina barrier; CD13: Aminopeptidase N; cGAMP: Cyclic guanosine monophosphate–adenosine; cGAS: Cyclic GMP-AMP synthase; IgG: Immunoglobulin G; LSCI: Laser speckle contrast imaging; LV: Lentiviral vectors; mRNA: messenger RNA; MTX: Methotrexate; NG2: Neural/glial antigen 2; PBS: phosphate buffered saline; PDGFR-β: platelet-derived growth factor receptor beta; PFA: paraformaldehyde; qRT-PCR: Quantitative Reverse Transcriptase-Polymerase Chain Reaction; RBF: Relative blood flow; RFC1: Reduced Folate Carrier 1; RIPA: Radioimmunoprecipitation assay; RPE: retinal pigmented epithelium; siRNA: short interfering RNA; SLC19a1:solute carrier family 19 (folate transporter), member 1; SNPs: single nucleotide polymorphisms; STING: stimulator of interferon genes; UV: ultraviolet; ZO-1: Zonula occludens 1

Competing interests

The authors declare that they have no competing interests.

Authors' contributions

GG contributed to the study design, performed surgeries and experiments, obtained tissues, performed immunohistochemistry, collected images and data, analyzed the data, prepared figures, wrote the draft of the manuscript and contributed to editing. GU contributed to the in vivo application of retinal ischemia model, retinal trypsin digestions and intravitreal injections, and writing of the paper. NB contributed to design and execution of Western Blottings and collected membrane images. MSB

contributed to design and execution of qRT-PCR experiments and performed related analysis. MCB designed and synthesized the lentiviral vector and performed cell-line Western Blottings. EK provided lentiviral vector as a courtesy and contributed to editing. MY acquired funds and administered the project, coordinated, and supervised the work, wrote the manuscript, and contributed to figures and edited the paper. All authors read and approved the final manuscript and provided minor modifications.

Data availability

All the data analyzed in this study, including raw data, are provided in this published article and the supplementary information files. There are no restrictions on data availability. Source data are provided with this paper.

Supplementary information is available for this paper.

Correspondence and requests for materials should be addressed to MY or GG.

REFERENCES

1. London, A., I. Benhar, and M. Schwartz, *The retina as a window to the brain-from eye research to CNS disorders.* Nat Rev Neurol, 2013. **9**(1): p. 44-53.
2. Cunha-Vaz, J., R. Bernardes, and C. Lobo, *Blood-retinal barrier.* Eur J Ophthalmol, 2011. **21 Suppl 6**: p. S3-9.
3. Kaur, C., W.S. Foulds, and E.A. Ling, *Blood-retinal barrier in hypoxic ischaemic conditions: basic concepts, clinical features and management.* Prog Retin Eye Res, 2008. **27**(6): p. 622-47.
4. Yemisci, M., et al., *Pericyte contraction induced by oxidative-nitrative stress impairs capillary reflow despite successful opening of an occluded cerebral artery.* Nature Medicine, 2009. **15**(9): p. 1031-U82.
5. Peppiatt, C.M., et al., *Bidirectional control of CNS capillary diameter by pericytes.* Nature, 2006. **443**(7112): p. 700-704.
6. Gursoy-Ozdemir, Y., M. Yemisci, and T. Dalkara, *Microvascular protection is essential for successful neuroprotection in stroke.* J Neurochem, 2012. **123 Suppl 2**: p. 2-11.
7. Dalkara, T., L. Alarcon-Martinez, and M. Yemisci, *Pericytes in Ischemic Stroke.* Adv Exp Med Biol, 2019. **1147**: p. 189-213.
8. Dalkara, T., Alarcon-Martinez L.,Yemisci M., *Role of Pericytes in Neurovascular Unit and Stroke*, in *Non-Neuronal Mechanisms of Brain Damage and Repair After Stroke*, J.C.e.a. (eds.), Editor. 2016, Springer International Publishing: Switzerland.
9. Wang, Y., et al., *Localization of the murine reduced folate carrier as assessed by immunohistochemical analysis.* Biochim Biophys Acta, 2001. **1513**(1): p. 49-54.
10. Hinken, M., et al., *Subcellular localization and distribution of the reduced folate carrier in normal rat tissues.* Eur J Histochem, 2011. **55**(1): p. e3.
11. Alam, C., et al., *Regulation of Reduced Folate Carrier (RFC) by Vitamin D Receptor at the Blood-Brain Barrier.* Molecular Pharmaceutics, 2017. **14**(11): p. 3848-3858.
12. Alam, C., et al., *Upregulation of reduced folate carrier by vitamin D enhances brain folate uptake in mice lacking folate receptor alpha.* Proc Natl Acad Sci U S A, 2019. **116**(35): p. 17531-17540.
13. He, L., et al., *Analysis of the brain mural cell transcriptome.* Sci Rep, 2016. **6**: p. 35108.
14. Naggar, H., et al., *Downregulation of reduced-folate transporter by glucose in cultured RPE cells and in RPE of diabetic mice.* Invest Ophthalmol Vis Sci, 2002. **43**(2): p. 556-63.

15. Naggar, H., et al., *Regulation of reduced-folate transporter-1 (RFT-1) by homocysteine and identity of transport systems for homocysteine uptake in retinal pigment epithelial (RPE) cells.* Exp Eye Res, 2003. **77**(6): p. 687-97.
16. Bridges, C.C., et al., *Transcellular transfer of folate across the retinal pigment epithelium.* Curr Eye Res, 2002. **24**(2): p. 129-38.
17. Smith, S.B., et al., *Regulation of the reduced-folate transporter by nitric oxide in cultured human retinal pigment epithelial cells.* Biochem Biophys Res Commun, 1999. **257**(2): p. 279-83.
18. Hosoya, K., K. Fujita, and M. Tachikawa, *Involvement of reduced folate carrier 1 in the inner blood-retinal barrier transport of methyltetrahydrofolate.* Drug Metab Pharmacokinet, 2008. **23**(4): p. 285-92.
19. Macosko, E.Z., et al., *Highly Parallel Genome-wide Expression Profiling of Individual Cells Using Nanoliter Droplets.* Cell, 2015. **161**(5): p. 1202-1214.
20. Fortelny, N., et al., *Can we predict protein from mRNA levels?* Nature, 2017. **547**(7664): p. E19-E20.
21. Alarcon-Martinez, L., et al., *Capillary pericytes express alpha-smooth muscle actin, which requires prevention of filamentous-actin depolymerization for detection.* Elife, 2018. **7**.
22. Alarcon-Martinez, L., et al., *Retinal ischemia induces alpha-SMA-mediated capillary pericyte contraction coincident with perivascular glycogen depletion.* Acta Neuropathol Commun, 2019. **7**(1): p. 134.
23. Cho, Y., et al., *Association of reduced folate carrier-1 (RFC-1) polymorphisms with ischemic stroke and silent brain infarction.* PLoS One, 2015. **10**(2): p. e0115295.
24. Grapp, M., et al., *Choroid plexus transcytosis and exosome shuttling deliver folate into brain parenchyma.* Nat Commun, 2013. **4**: p. 2123.
25. Alam, C., et al., *Nuclear respiratory factor 1 (NRF-1) upregulates the expression and function of reduced folate carrier (RFC) at the blood-brain barrier.* FASEB J, 2020. **34**(8): p. 10516-10530.
26. Alqarni, A.M. and M.P. Zeidler, *How does methotrexate work?* Biochem Soc Trans, 2020. **48**(2): p. 559-567.
27. Wright, N.J., et al., *Methotrexate recognition by the human reduced folate carrier SLC19A1.* Nature, 2022. **609**(7929): p. 1056-1062.
28. Luteijn, R.D., et al., *SLC19A1 transports immunoreactive cyclic dinucleotides.* Nature, 2019. **573**(7774): p. 434-438.
29. Ritchie, C., et al., *SLC19A1 Is an Importer of the Immunotransmitter cGAMP.* Mol Cell, 2019. **75**(2): p. 372-381 e5.
30. Karatas, H., et al., *Thrombotic distal middle cerebral artery occlusion produced by topical FeCl(3) application: a novel model suitable for intravital microscopy and thrombolysis studies.* J Cereb Blood Flow Metab, 2011. **31**(6): p. 1452-60.
31. Kureli, G., et al., *F-actin polymerization contributes to pericyte contractility in retinal capillaries.* Exp Neurol, 2020. **332**: p. 113392.
32. Hara, A., et al., *Folate antagonist, methotrexate induces neuronal differentiation of human embryonic stem cells transplanted into nude mouse retina.* Neurosci Lett, 2010. **477**(3): p. 138-43.
33. Discovery, H. *Accell™ siRNA References.* 2021 [cited 2022 01.09]; Available from: https://horizondiscovery.com/-/media/Files/Horizon/resources/Reading-lists/accell-sirna-ref-reading.pdf.
34. Taniguchi, T., et al., *Novel use of a chemically modified siRNA for robust and sustainable in vivo gene silencing in the retina.* Sci Rep, 2020. **10**(1): p. 22343.
35. Calkins, D.J., et al., *Biodistribution of intravitreal (lenadogene) nolparvovec gene therapy in nonhuman primates.* Mol Ther Methods Clin Dev, 2021. **23**: p. 307-318.

36. Yu-Wai-Man, P., et al., *Bilateral visual improvement with unilateral gene therapy injection for Leber hereditary optic neuropathy.* Sci Transl Med, 2020. **12**(573).
37. Beker, M., et al., *Lentivirally administered glial cell line-derived neurotrophic factor promotes post-ischemic neurological recovery, brain remodeling and contralesional pyramidal tract plasticity by regulating axonal growth inhibitors and guidance proteins.* Exp Neurol, 2020. **331**: p. 113364.
38. Chou, J.C., S.D. Rollins, and A.A. Fawzi, *Trypsin digest protocol to analyze the retinal vasculature of a mouse model.* J Vis Exp, 2013(76): p. e50489.
39. Kuwabara, T. and D.G. Cogan, *Studies of retinal vascular patterns. I. Normal architecture.* Arch Ophthalmol, 1960. **64**: p. 904-11.
40. Zudaire, E., et al., *A computational tool for quantitative analysis of vascular networks.* PLoS One, 2011. **6**(11): p. e27385.
41. Chancy, C.D., et al., *Expression and differential polarization of the reduced-folate transporter-1 and the folate receptor alpha in mammalian retinal pigment epithelium.* J Biol Chem, 2000. **275**(27): p. 20676-84.
42. Trippett, T.M., et al., *Localization of a human reduced folate carrier protein in the mitochondrial as well as the cell membrane of leukemia cells.* Cancer Res, 2001. **61**(5): p. 1941-7.
43. Torlakovic, E.E., et al., *Standardization of negative controls in diagnostic immunohistochemistry: recommendations from the international ad hoc expert panel.* Appl Immunohistochem Mol Morphol, 2014. **22**(4): p. 241-52.
44. Wei, Y., et al., *Nrf2 in ischemic neurons promotes retinal vascular regeneration through regulation of semaphorin 6A.* Proc Natl Acad Sci U S A, 2015. **112**(50): p. E6927-36.
45. Auricchio, A., et al., *Exchange of surface proteins impacts on viral vector cellular specificity and transduction characteristics: the retina as a model.* Hum Mol Genet, 2001. **10**(26): p. 3075-81.
46. Wang, X., et al., *Blood brain barrier breakdown was found in non-infarcted area after 2-h MCAO.* J Neurol Sci, 2016. **363**: p. 63-8.
47. Chen, B., et al., *Severe blood-brain barrier disruption and surrounding tissue injury.* Stroke, 2009. **40**(12): p. e666-74.
48. Jin, X., et al., *Spatiotemporal evolution of blood brain barrier damage and tissue infarction within the first 3h after ischemia onset.* Neurobiol Dis, 2012. **48**(3): p. 309-16.
49. Geier, E.G., et al., *Profiling solute carrier transporters in the human blood-brain barrier.* Clin Pharmacol Ther, 2013. **94**(6): p. 636-9.
50. Zhao, R., et al., *Rescue of embryonic lethality in reduced folate carrier-deficient mice by maternal folic acid supplementation reveals early neonatal failure of hematopoietic organs.* J Biol Chem, 2001. **276**(13): p. 10224-8.
51. Petrus, P., et al., *Adipocyte Expression of SLC19A1 Links DNA Hypermethylation to Adipose Tissue Inflammation and Insulin Resistance.* J Clin Endocrinol Metab, 2018. **103**(2): p. 710-721.
52. Meyer, C.H., et al., *Routes for Drug Delivery to the Eye and Retina: Intravitreal Injections.* Dev Ophthalmol, 2016. **55**: p. 63-70.
53. Wang, X., et al., *Functional regulation of P-glycoprotein at the blood-brain barrier in proton-coupled folate transporter (PCFT) mutant mice.* FASEB J, 2013. **27**(3): p. 1167-75.
54. Yang, H., et al., *STING activation reprograms tumor vasculatures and synergizes with VEGFR2 blockade.* J Clin Invest, 2019. **129**(10): p. 4350-4364.
55. Al Ahmad, A., M. Gassmann, and O.O. Ogunshola, *Maintaining blood-brain barrier integrity: pericytes perform better than astrocytes during prolonged oxygen deprivation.* J Cell Physiol, 2009. **218**(3): p. 612-22.

56. Yang, T., et al., *Pericytes of Indirect Contact Coculture Decrease Integrity of Inner Blood-Retina Barrier Model In Vitro by Upgrading MMP-2/9 Activity.* Dis Markers, 2021. **2021**: p. 7124835.
57. Daneman, R., et al., *Pericytes are required for blood-brain barrier integrity during embryogenesis.* Nature, 2010. **468**(7323): p. 562-6.
58. Bell, R.D., et al., *Pericytes control key neurovascular functions and neuronal phenotype in the adult brain and during brain aging.* Neuron, 2010. **68**(3): p. 409-27.
59. Stallcup, W.B., *The NG2 Proteoglycan in Pericyte Biology.* Adv Exp Med Biol, 2018. **1109**: p. 5-19.
60. You, W.K., et al., *NG2 proteoglycan promotes tumor vascularization via integrin-dependent effects on pericyte function.* Angiogenesis, 2014. **17**(1): p. 61-76.
61. Narawa, T., et al., *Stereoselectivity of the reduced folate carrier in Caco-2 cells.* Chirality, 2005. **17**(8): p. 444-9.
62. Matherly, L.H. and Z. Hou, *Structure and function of the reduced folate carrier a paradigm of a major facilitator superfamily mammalian nutrient transporter.* Vitam Horm, 2008. **79**: p. 145-84.
63. O'Connor, C., et al., *Folate transporter dynamics and therapy with classic and tumor-targeted antifolates.* Sci Rep, 2021. **11**(1): p. 6389.
64. Ma, D., H. Huang, and J.A. Moscow, *Down-regulation of reduced folate carrier gene (RFC1) expression after exposure to methotrexate in ZR-75-1 breast cancer cells.* Biochem Biophys Res Commun, 2000. **279**(3): p. 891-7.
65. Lobo, E.D. and J.P. Balthasar, *Pharmacokinetic-pharmacodynamic modeling of methotrexate-induced toxicity in mice.* J Pharm Sci, 2003. **92**(8): p. 1654-64.
66. Hillcoat, B.L., J.P. Perkins, and J.R. Bertino, *Dihydrofolate reductase from the L1210 R murine lymphoma. Further studies on the binding of substrates and inhibitors to the enzyme.* J Biol Chem, 1967. **242**(20): p. 4777-81.
67. Hillcoat, B.L. and J.R. Bertino, *Vriation of dihydrofolate reductase activity in mammalian cells in vitro.* Exp Cell Res, 1969. **56**(2): p. 304-8.
68. Hsieh, Y.C., et al., *Species-specific differences in translational regulation of dihydrofolate reductase.* Mol Pharmacol, 2009. **76**(4): p. 723-33.
69. Liu, T., et al., *Tyrosine phosphorylation of HSC70 and its interaction with RFC mediates methotrexate resistance in murine L1210 leukemia cells.* Cancer Lett, 2015. **357**(1): p. 231-241.
70. Dattilo, M., N.J. Newman, and V. Biousse, *Acute retinal arterial ischemia.* Ann Eye Sci, 2018. **3**.
71. Andreeva, K., et al., *Time-dependent Gene Profiling Indicates the Presence of Different Phases for Ischemia/Reperfusion Injury in Retina.* Ophthalmol Eye Dis, 2014. **6**: p. 43-54.
72. Abcouwer, S.F., et al., *Effects of ischemic preconditioning and bevacizumab on apoptosis and vascular permeability following retinal ischemia-reperfusion injury.* Invest Ophthalmol Vis Sci, 2010. **51**(11): p. 5920-33.
73. Yang, C., et al., *Ischemia-Reperfusion Injury Reduces Kidney Folate Transporter Expression and Plasma Folate Levels.* Front Immunol, 2021. **12**: p. 678914.
74. Assaraf, Y.G., *The role of multidrug resistance efflux transporters in antifolate resistance and folate homeostasis.* Drug Resist Updat, 2006. **9**(4-5): p. 227-46.

Supplemental Figure 1

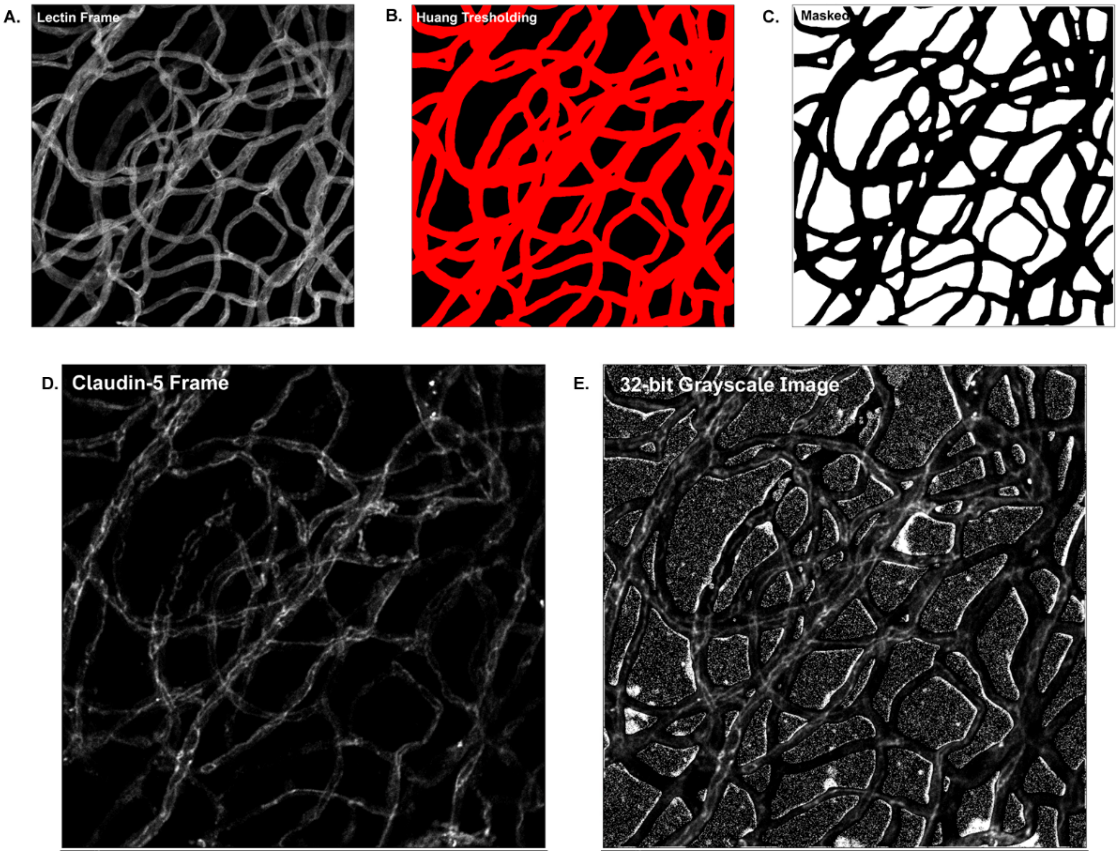

Supplemental Figure 1. Representative consecutive pictures displaying the method used for the quantitative assessment of confocal images of retinal trypsin digest preparations with ImageJ. A) Double stained images exported as RAW 8-bit grayscale .tiff formats and opened in ImageJ with lectin frame belonging to each image filtered by Gaussian blur (sigma=4) to reduce the random noise that overlapped with microvessel signal. B) Huang Thresholding was applied to mask lectin positive microvessel area of the particular image. C) Masked image that was de-speckled (Process tab>Noise>Despeckle) and eroded (Process tab>Binary>Erode), to result the binary image divided by 255 using Math function (Process tab>Math>Divide) and converted microvessel pixels to "1" and background pixels to "0". D) "RAW" overlapping grayscale image belonging to tight junctions (for this example claudin-5) divided by the binary. E) The 32-bit grayscale image which microvessels having the original intensity and with the infinite background were obtained by mean grey value (RFU, range between 0-255) providing the mean intensity of the pixels which occupied the microvessel area.

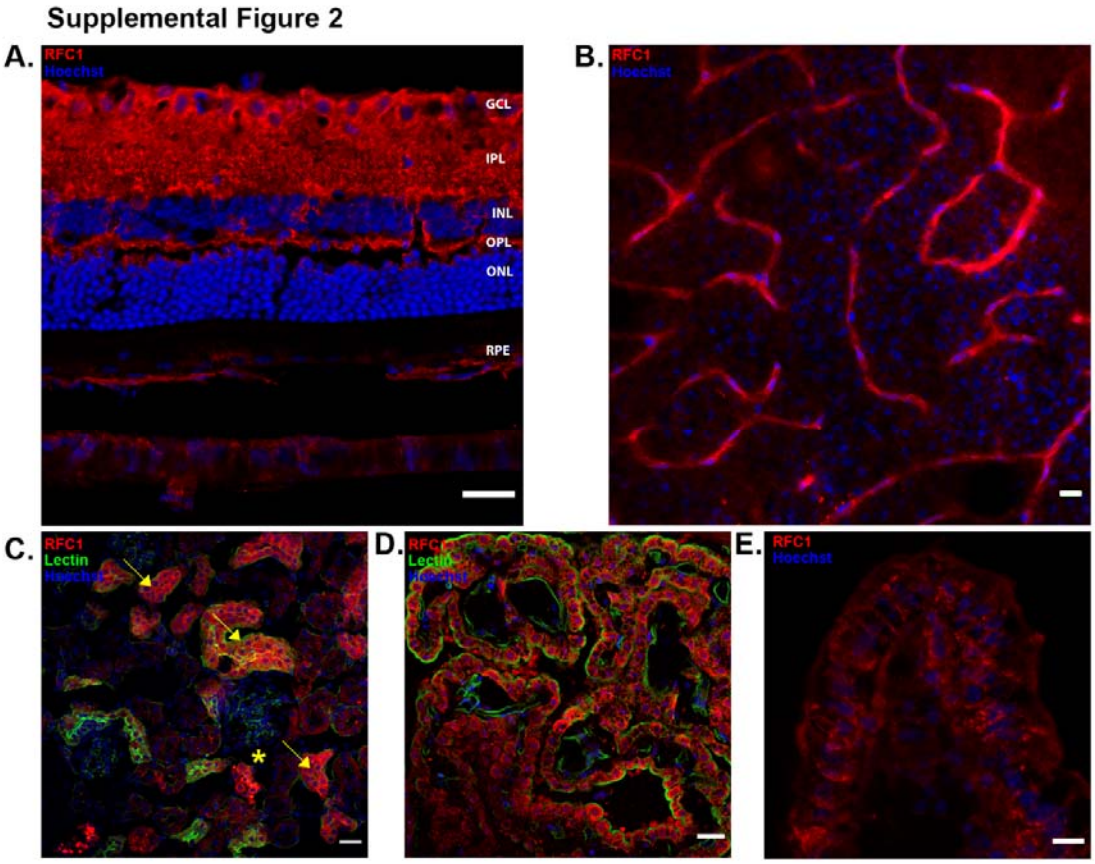

Supplemental Figure 2. RFC1 immunostaining of the adult mouse retina. A) Ex-vivo labeling of 20 µm coronal cryo-section from PFA fixated eyeballs of naïve Swiss Albino mice with anti-RFC1 antibody (red). Abundant RFC1 immunopositivity is observed along ganglion cell layer (GCL), inner plexiform layer (IPL), outer plexiform layer (OPL) where retinal microvessels forms vascular horizontal vascular beds. However, this preparation limited the observation of microvessels, hence inner BRB, as it commonly included microvessels circularly rather than longitudinally. The retinal pigment epithelium (RPE) which is known to express RFC1 previously is well stained with anti-RFC1 antibody (red) as our positive control. Scale Bar=25 µm. B) The microvessels constituting inner BRB form the deep vascular plexus of the retina were immunohistochemically labelled with anti-RFC1 antibody in PFA fixated whole-mount retinas. C) The proximal tubules of mouse kidney (yellow arrows), D) ependymal cells of choroid plexus, and E) epithelia of ileum served as positive controls for immunohistochemical labeling of RFC1 (red), as they known to express RFC1 abundantly. Of note (asterisk in C), glomeruli that comprise microvessels had no RFC1 signal, hence validated the immunohistochemical labelling. Nuclei were labeled with Hoechst 33258 (blue), and vessels by lectin (green). Scale bars=25 µm (C); 10 µm (D-E).

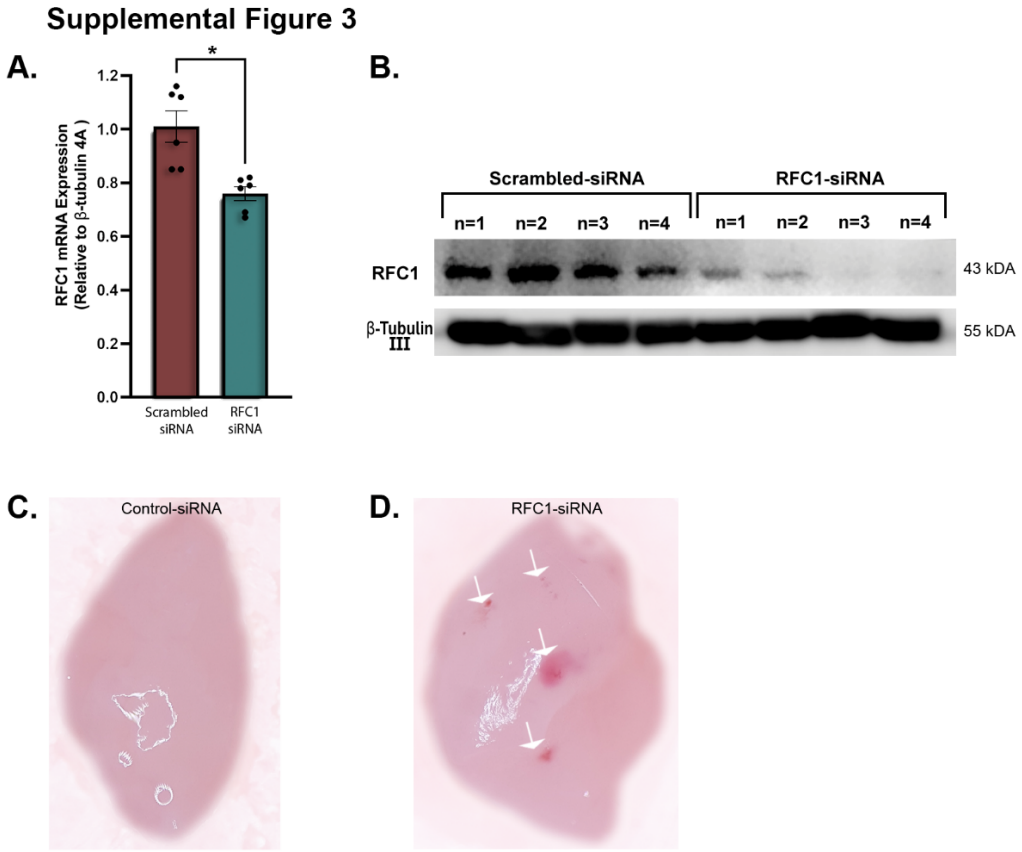

Supplemental Figure 3. Accell siRNA mediated RFC1 knockdown *in vivo*. A) The graph shows that RFC1-siRNA delivery reduced retinal RFC1 mRNA levels by 24.75% when compared to scrambled-siRNA (*p=0.004) (n=3, dots represent double technical replications). Results represented as mean ± S.E.M. B) Western blotting image of retinas (n=8 mice) depicting robust decrease in RFC1 protein of RFC1-siRNA delivered ones compared to scrambled-siRNA. β-Tubulin III was loading control. 35 µg protein was loaded for each retina. C, D) Representative images of retinas observed under stereomicroscope where RFC1-siRNA treated fragile retinas had patchy hemorrhages (white arrows) indicating disintegration of blood vessels when compared to scramble-siRNA treated intact retina.

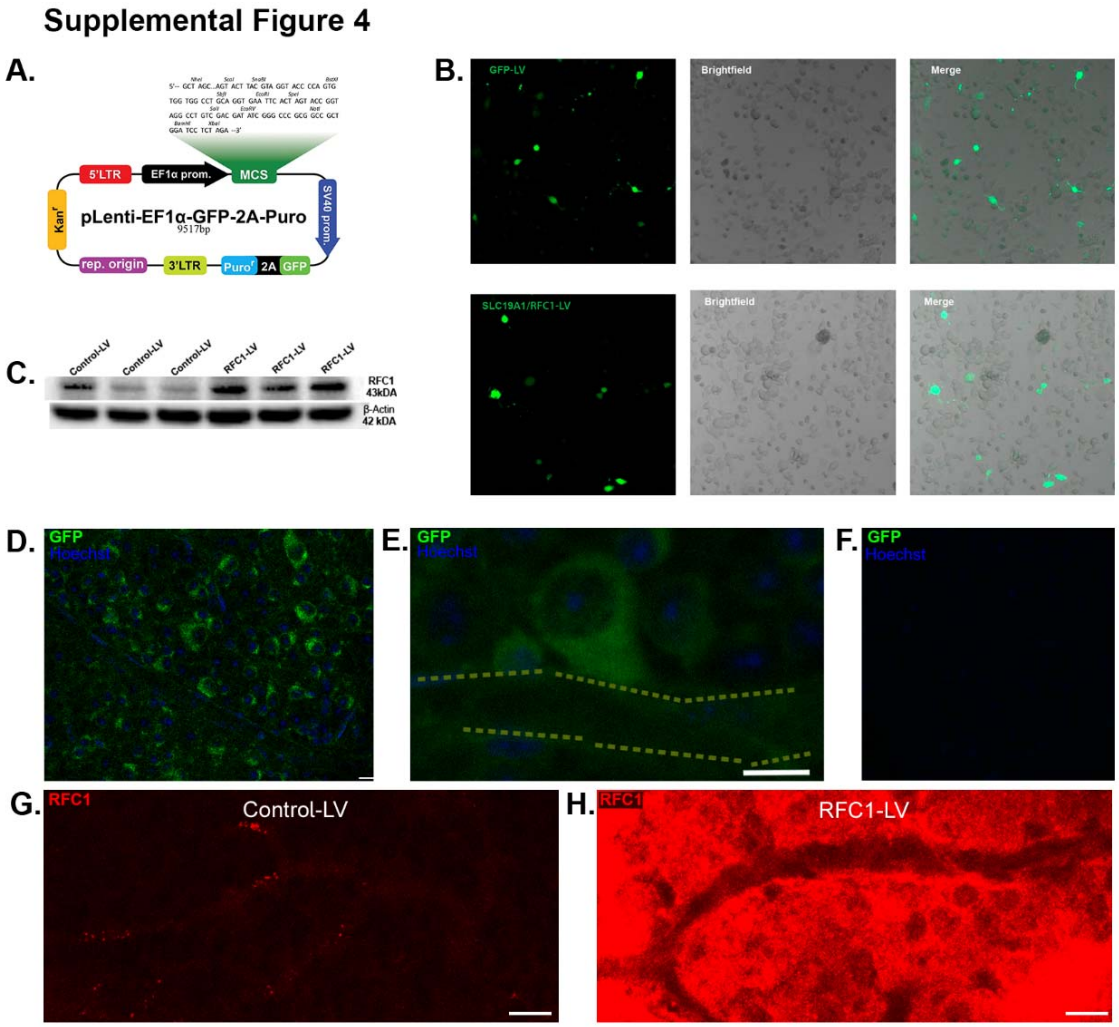

Supplemental Figure 4. Lentiviral vector-mediated overexpression of RFC1 protein *in vitro* and *in vivo*. A) The figure shows pLenti-EF1α-GFP-2A-Puro backbone, into which RFC1 gene was cloned. The promoter was elongation factor-1 alpha (EF1α), which is one of the strongest promoters in mammalian cells, and the reporter gene was GFP. B) The images obtained via fluorescence and brightfield microscopy showed GFP expression (green) after in vitro delivery into the neuroblastoma cell line (N2a). C) The Western Blotting image shows corresponding overexpression of RFC1 protein in RFC1-LV transduced neuroblastoma cells (N2a) compared to Control-LV transduced cells. For cell culture lysates, Beta-Actin was the loading control. D) The confocal images from whole mount retinas confirmed the intravitreal delivery of LV-RFC1 or Control-LV into the mouse eye showing lentiviral vectors infected various retinal cells, as reporter gene GFP (green) signal indicated. E) Also, as magnified image showed, perivascular cells and pericytes expressed GFP protein in LV-RFC1 or Control-LV injected retinas, microvessel trace was shown by dashed line. F) Naïve retina image

showed no green fluorescence. H, I) The representative images of whole mount retinas which had been treated by LV-RFC1 showed increased RFC1 immunosignal (red) compared to Control-LV injected control retinas (n=3). Nuclei were labelled with Hoechst 33258 (blue). Data are mean ± S.E.M. Scale bar=10 μm

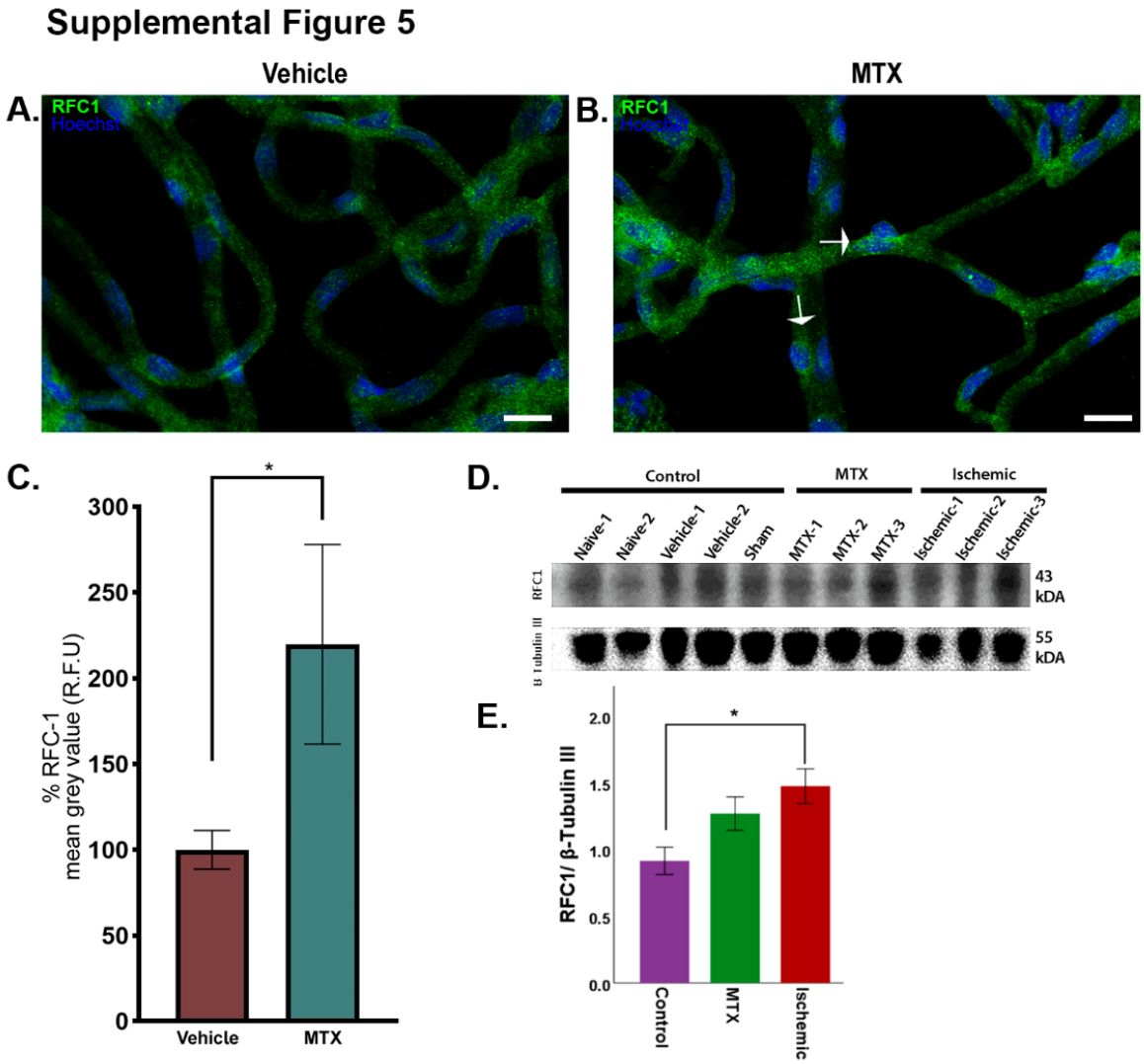

Supplemental Figure 5. Methotrexate (MTX) increased RFC1 levels in adult mouse retina as well as ischemia. A, B) The image of retinal microvessels obtained by retinal trypsin digestion that were immunohistochemically labelled with anti-RFC1 antibody. RFC1 immunosignal increased in microvessels in one dose intravitreal MTX delivery group (n=4) compared to vehicle (n=4). The arrows showed that pericyte contacting microvessel segments showed further immunosignal increase in RFC1 immunosignal (green). C) The graph shows that MTX delivery significantly augmented the mean grey value of RFC1 (*p= 0.0427; n=3). D) The representative Western blotting image from

Naïve (n=2), vehicle (n=2) or MTX (n=3), and ischemic (n=3) retinas. Housekeeping gene β-Tubulin III was used as loading control. E) The graph shows the relative density measurements of bands which were calculated by proportioning to loading control. One hour permanent retinal ischemia increased relative RFC1 protein levels compared to control. Nuclei were labelled with Hoechst 33258 (blue). Data are mean ± S.E.M. Mann-Whitney U; Scale bar: 10 μm.

Figure 1

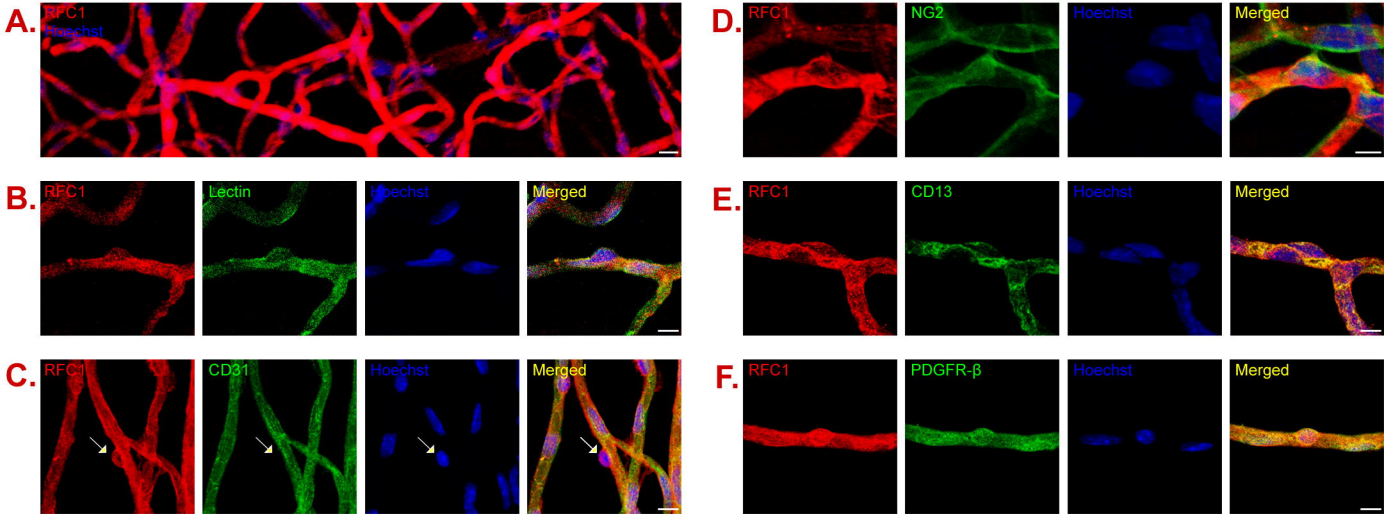
A.
RFC1
Hoechst
B.
RFC1
Lectin
Hoechst
Merged
C.
RFC1
CD31
Hoechst
Merged
D.
RFC1
NG2
Hoechst
Merged
E.
RFC1
CD13
Hoechst
Merged
F.
RFC1
PDGFR-β
Hoechst
Merged

Figure 2

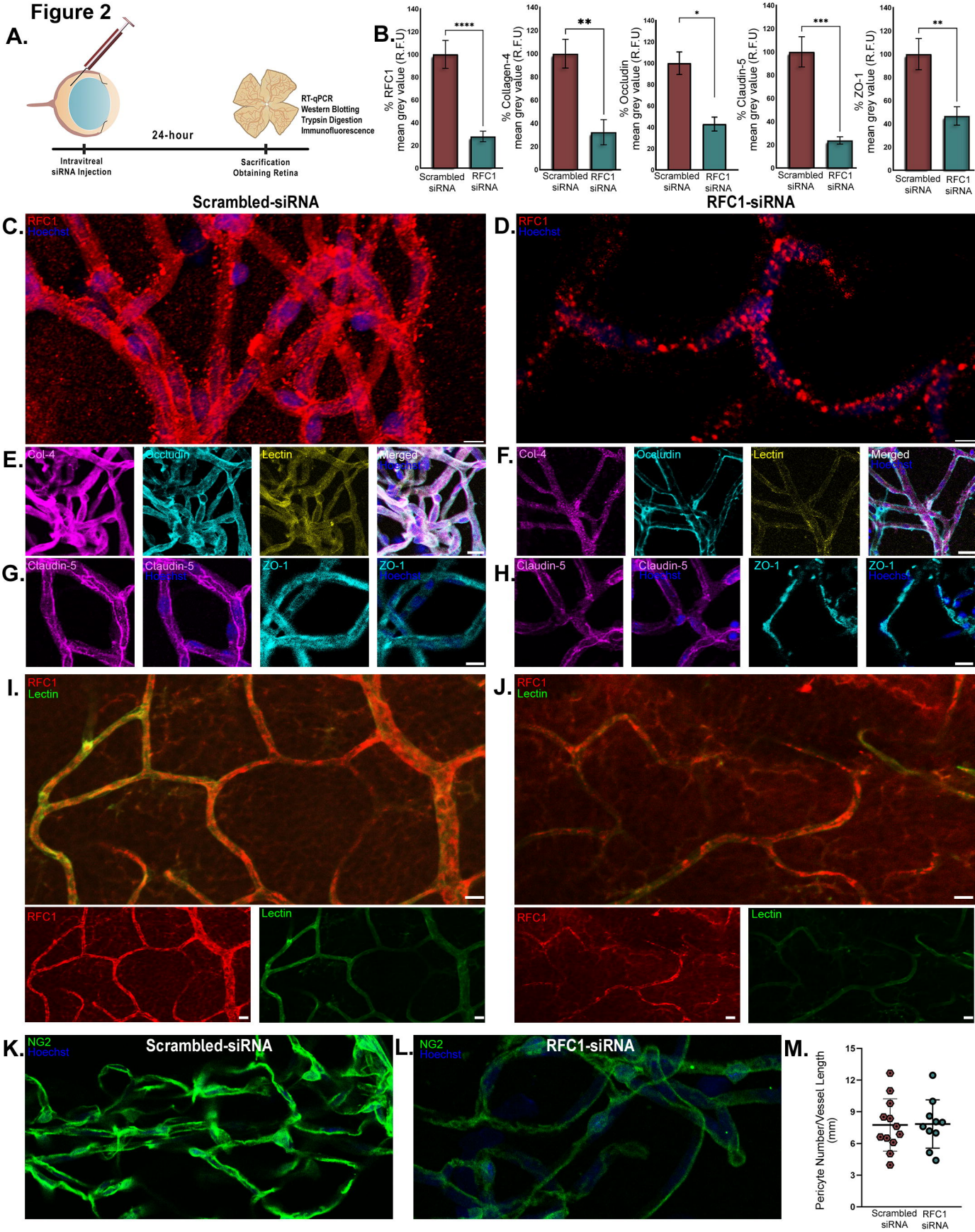
A.
24-hour
Intravitreal siRNA Injection
Sacrification Obtaining Retina
RT-qPCR
Western Blotting
Trypsin Digestion
Immunofluorescence
B.
% RFC1 mean grey value (R.F.U)
% Collagen-4 mean grey value (R.F.U)
% Occludin mean grey value (R.F.U)
% Claudin-5 mean grey value (R.F.U)
% ZO-1 mean grey value (R.F.U)
Scrambled siRNA
RFC1 siRNA
Scrambled-siRNA
RFC1-siRNA
C.
D.
RFC1
Hoechst
E.
F.
Col-4
Occludin
Lectin
Merged
G.
H.
Claudin-5
ZO-1
I.
J.
RFC1
Lectin
K.
L.
NG2
M.
Pericyte Number/Vessel Length (mm)

Figure 3

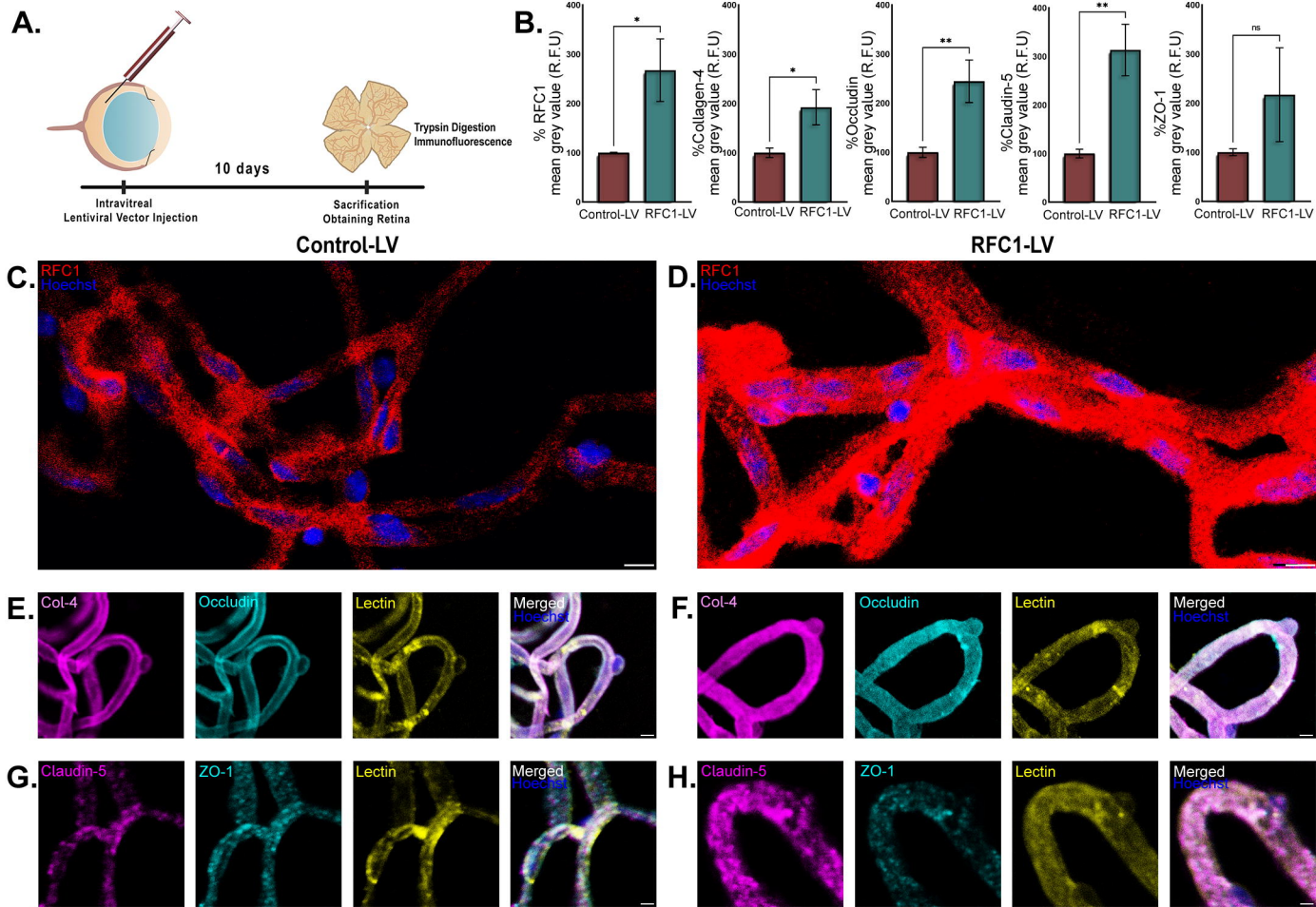
A.
10 days
Intravitreal
Lentiviral Vector Injection
Trypsin Digestion
Immunofluorescence
Sacrification
Obtaining Retina
B.
% RFC1
mean grey value (R.F.U)
%Collagen-4
mean grey value (R.F.U)
%Occludin
mean grey value (R.F.U)
%Claudin-5
mean grey value (R.F.U)
%ZO-1
mean grey value (R.F.U)
Control-LV
RFC1-LV
ns
Control-LV
RFC1-LV
C.
D.
RFC1
Hoechst
E.
F.
G.
H.
Col-4
Occludin
Lectin
Merged
Hoechst
Claudin-5
ZO-1

Figure 4

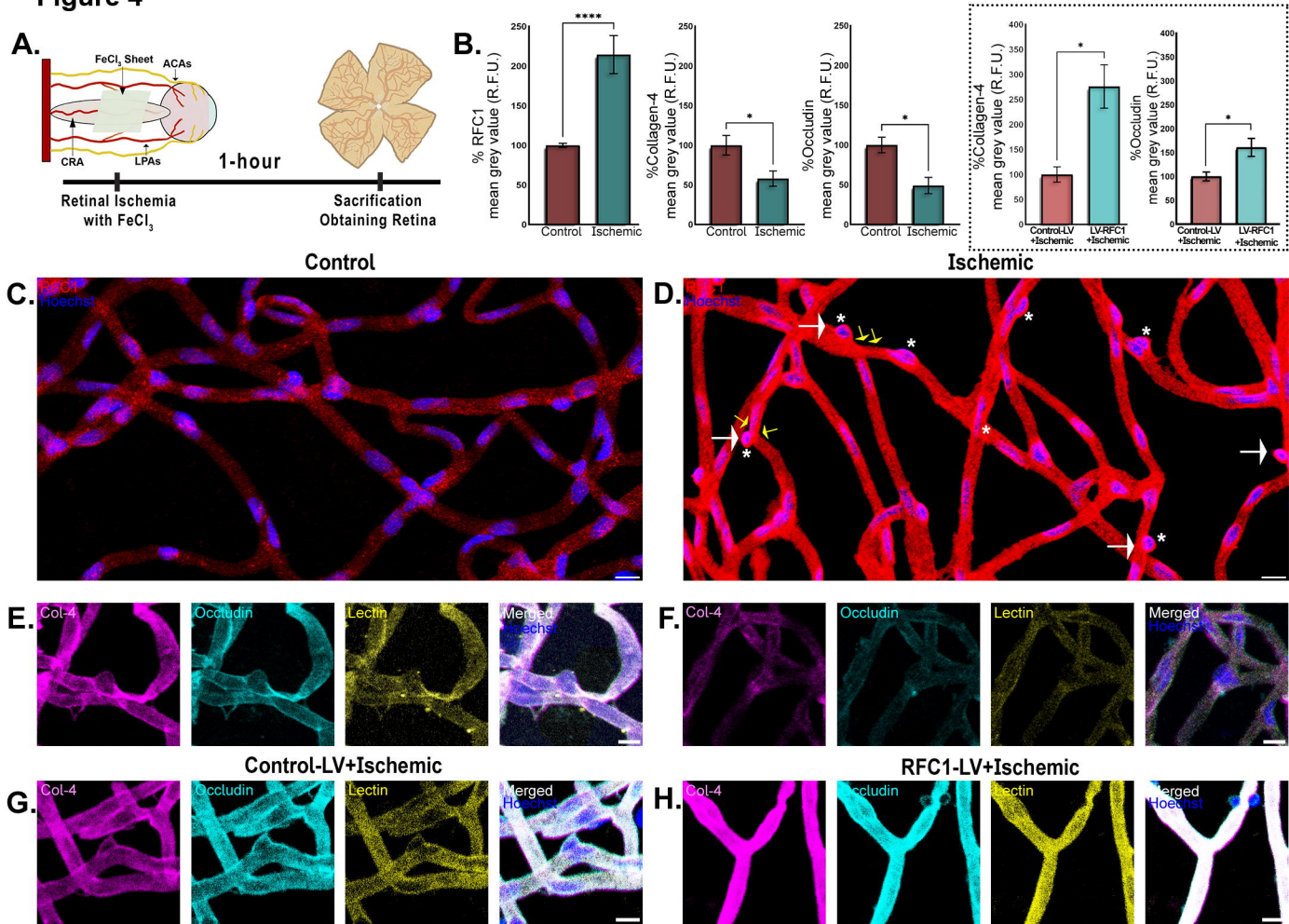
A.
FeCl3 Sheet
ACAs
CRA
LPAs
1-hour
Retinal Ischemia with FeCl3
Sacrification Obtaining Retina
B.
% RFC1 mean grey value (R.F.U.)
%Collagen-4 mean grey value (R.F.U.)
%Occludin mean grey value (R.F.U.)
Control
Ischemic
Control-LV +Ischemic
LV-RFC1 +Ischemic
Control
Ischemic
C.
D.
Col-4
Hoechst
E.
F.
Occludin
Lectin
Merged
Control-LV+Ischemic
RFC1-LV+Ischemic
G.
H.

Figure 5

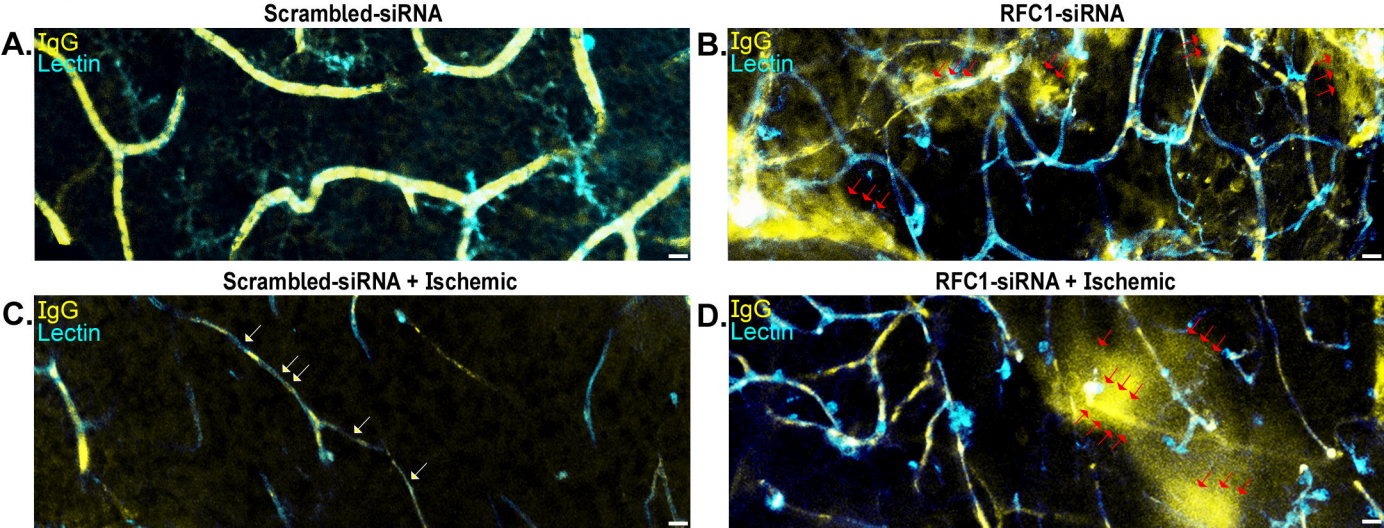
Scrambled-siRNA
A.
IgG
Lectin
RFC1-siRNA
B.
IgG
Lectin
Scrambled-siRNA + Ischemic
C.
IgG
Lectin
RFC1-siRNA + Ischemic
D.
IgG
Lectin